NASA
Technical
Paper
2319

July 1984

Chemical Mechanisms and Reaction Rates for the Initiation of Hot Corrosion of IN-738

George C. Fryburg,
Fred J. Kohl,
and Carl A. Stearns

NASA

NASA Technical Paper 2319

1984

Chemical Mechanisms and Reaction Rates for the Initiation of Hot Corrosion of IN-738

George C. Fryburg,
Fred J. Kohl,
and Carl A. Stearns

Lewis Research Center
Cleveland, Ohio

National Aeronautics
and Space Administration

Scientific and Technical Information Branch

Summary

Sodium-sulfate-induced hot corrosion of preoxidized IN-738 was studied at 975° C with special emphasis on the processes occurring during the long induction period. Thermogravimetric tests were run for predetermined periods of time, and then one set of specimens was washed with water. Chemical analysis of the wash solutions yielded information about water-soluble metal salts and residual sulfate. A second set of samples was cross sectioned dry and polished in a nonaqueous medium. Element distributions within the oxide scale were obtained from electron microprobe X-ray micrographs. Evolution of SO_2 was monitored during the thermogravimetric tests. Kinetic rate studies were performed for several pertinent processes; appropriate rate constants were obtained for the following chemical reactions:

$$Cr_2O_3 + 2\ Na_2SO_4(l) + 3/2\ O_2 \rightarrow 2\ Na_2CrO_4(l) + 2\ SO_3(g)$$

$$n\ TiO_2 + Na_2SO_4(l) \rightarrow Na_2O(TiO_2)_n + SO_3(g)$$

$$n\ TiO_2 + Na_2CrO_4(l) \rightarrow Na_2O(TiO_2)_n + CrO_3(g)$$

Introduction

Nickel-base alloys are used extensively in gas turbine engine components because of their superior mechanical properties. However, these superalloys are generally susceptible to a form of environmental attack known as hot corrosion. Hot corrosion is encountered under circumstances where Na_2SO_4 is deposited from the combustion gases onto the hot-gas-path parts, especially the turbine blades and vanes. This corrosion has been a serious problem for many years in aircraft engines and also in marine engines and land-based power generating systems. It is believed that the problem will be aggravated by the anticipated use of higher operating temperatures and pressures in future gas turbine engines. Further contributions can be expected from the increased use of cheaper, "dirtier" fuels. Therefore it is desirable to obtain a clearer understanding of the chemical processes involved in the hot corrosion of these superalloys.

Recently we reported on the chemical reactions involved in the initiation of hot corrosion of the alloys B-1900 and NASA-TRW VIA (ref. 1). These are nickel-base alloys that derive their oxidation resistance from the formation of a thin, dense, continuous oxide layer composed largely of α-Al_2O_3. Hot corrosion was induced by coating metal samples with Na_2SO_4 and oxidizing them at higher temperatures. Thermogravimetric tests were performed and SO_2 evolution was monitored. Additional information about the chemical reactions occurring was obtained from chemical analysis of wash solutions and from energy dispersive X-ray analysis of the oxide scales of specimens that were corroded for predetermined periods of time. It was shown that, after an induction period, hot corrosion caused basic fluxing of the protective Al_2O_3 layer by the liquid Na_2SO_4 deposit. This was followed by a catastrophic rate of attack resulting from an acidic fluxing of the remaining oxide layer by a Na_2MoO_4-MoO_3 molten phase that had formed underneath the oxide layer.

Unlike B-1900 and VIA, the alloy IN-738 derives its oxidation resistance from a protective layer composed largely of Cr_2O_3. This superalloy is of special interest because of its present wide use, both coated and uncoated, in gas turbine engines (refs. 2 and 3). This position of prominence is due not only to its good mechanical properties, but also to its superior hot corrosion resistance.

The Na_2SO_4-induced hot corrosion of IN-738 in the temperature range 825° to 1000° C has been studied by a number of investigators using a variety of experimental techniques (refs. 3 to 13). The results have shown that either the alloy did not display hot corrosion at all under the test conditions, or the hot corrosion was preceded by a long induction period during which the corrosion rate was similar to that in simple oxidation. Most of these studies have emphasized the kinetics of the hot corrosion, usually in comparison with other alloys, or the morphology of the corrosion scale. Less effort has been devoted to the important processes that must be occurring during the long induction period. We have investigated the Na_2SO_4-induced hot corrosion of IN-738 at 975° C with special emphasis on the chemical and

physical processes occurring during the induction period, processes that lead to the initiation of catastrophic hot corrosion attack of this alloy. We have used the same techniques that were employed in our studies of B-1900 and VIA as described in reference 1. In addition, we have performed rate studies on several of the simple processes suspected of being important in the hot corrosion of IN-738. Recently we reported the effects of temperature and oxide scale thickness on the hot corrosion of IN-738 (ref. 13). Those results complement the present work, which emphasizes chemical processes.

Experimental Procedure

Specimens of alloy IN-738 were obtained from commercial sources and given conventional heat treatments. The composition of the alloy is presented in table I. Test samples typically measured 0.3 × 1.0 × 2.5 cm and had a 0.3-cm-diameter hangdown hole in one end. All surfaces were glass-bead blasted to give a uniform matte finish. The samples were cleaned ultrasonically in trichloroethylene, detergent, distilled water, acetone, and ethanol and then dried in an oven at 120° C.

All samples were preoxidized at 975° C in 1 atm of slowly flowing oxygen for 24 hr. Hot corrosion was induced by coating the preoxidized samples with about 3 mg cm^{-2} of Na_2SO_4 followed by isothermal oxidation at 975° C. The Na_2SO_4 was applied by air brushing a saturated solution of Na_2SO_4 onto the specimen, which was heated on a hotplate to 200° C. The salt-coated specimens were oxidized in a vertical tube furnace. Oxygen flowed downward at 126 cm min^{-1} (620 milliliters min^{-1}) in the 2.5-cm-diameter quartz furnace tube. The specimen under test was suspended in the tube on a Pt-20Rh alloy chain. Continuous weight measurements were made with a Cahn R-100 microbalance. The recorded weight changes were corrected for flow and buoyancy effects. Drs. Reza Haque and Ajay K. Misra ran some of the hot corrosion tests.

TABLE I.—COMPOSITION OF IN-738

Element	Concentration	
	wt %	at. %
Nickel	61.5	59
Chromium	16.0	17.5
Aluminum	3.4	7.2
Titanium	3.4	4.0
Cobalt	8.5	8.2
Molybdenum	1.7	1.0
Tungsten	2.6	.8
Tantalum	1.7	.6
Niobium	.9	.6
Zirconium	.1	.06
Carbon	.17	.81

The concentration of SO_2 in the gas flowing out of the furnace tube was measured continuously during the test with a ThermoElectron pulsed fluorescent analyzer that is specific to SO_2. The detection capability extended from 0.01 to 50 ppm. The effluent from the furnace tube was conducted into the SO_2 analyzer through stainless steel fittings and Teflon tubing.

Samples were run for predetermined periods of time and then cooled to room temperature. One set of samples was mounted and cross sectioned for morphological examination of the corrosion scale by light microscopy and electron microprobe techniques. These samples were coated with copper in an electron beam evaporator before they were mounted and were cross sectioned dry over an 8-hr period. The samples were polished in Varsol to prevent removal of water-soluble compounds. The microprobe data were obtained by Mr. Frank M. Terepka. Reaction products were identified from elemental X-ray micrographs and X-ray diffraction analyses reported previously (ref. 7). A second set of samples was washed with water to extract soluble species. Each specimen was treated for 15 min in 50 milliliters of hot water, and the resulting solutions were analyzed for metal cations or anions by atomic absorption techniques. Residual sulfate was determined by ion chromatography. The chemical analyses were performed by Mr. Warren F. Davis and Ms. Constance S. Buchar.

Results and Discussion

The hot corrosion specimens used in this investigation were all preoxidized in oxygen for 24 hr at 975° C. The isothermal oxidation of IN-738 was essentially parabolic at this temperature; a typical specific weight gain curve is presented in figure 1. The 24-hr preoxidation treatment effected a weight gain of 1.7 mg cm^{-2} and produced a

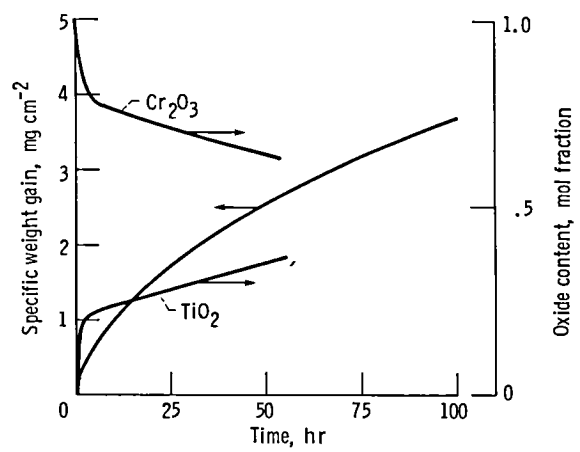

Figure 1.—Typical specific weight gain as a function of time for isothermal oxidation of IN-738 at 975° C in flowing oxygen and with mol fraction of Cr_2O_3 and TiO_2 in scale.

10-μm-thick oxide scale on the sample. Elemental X-ray micrographs of a typical oxide layer are presented in figure 2. The oxide was composed primarily of Cr_2O_3 with considerable amounts of TiO_2 associated with it. Tentacle-like internal oxides, which were essentially Al_2O_3, were observed below the Cr_2O_3 layer, extending an additional 30 μm into the substrate. In addition, an oxide of tantalum and possibly niobium lay scattered along the lower edge of the 10-μm-thick Cr_2O_3–TiO_2 layer. Titanium exhibited a marked depletion zone about 30 μm thick, and chromium showed a less marked zone of about the same thickness. Little or no nickel or molybdenum appeared in the oxide layer.

These results are in general agreement with our previous results for specimens oxidized in oxygen for 100 hr at 900° and 1000° C (ref. 14). There is one difference: the specimens oxidized for the longer time (100 hr) exhibited a definite layer of TiO_2 on top of the Cr_2O_3–TiO_2 layer. This was not observed on the present (24 hr) samples, where the TiO_2 appeared to be only intermixed with the Cr_2O_3. In situ high-temperature X-ray diffraction was performed to identify the oxides formed during isothermal oxidation. With this technique (ref. 15) the course of oxidation reactions can be followed at temperature, and the relative amounts of the oxides can be roughly calculated. The results for Cr_2O_3 and TiO_2 are presented in figure 1 as mol fractions at various times, and they show that the oxide layer formed in 24 hr was about 75-mol% Cr_2O_3 and 25-mol% TiO_2.

Thick scales formed on IN–738 during oxidation tend to spall upon cooling to room temperature, but this was not usually a problem with our samples because the oxide scale was only 10 μm thick. The preoxidation extended the length of the induction period observed during induced hot corrosion, and it produced a sample that was characterizeable and fairly stable to further oxidation, the rate after 24 hr of oxidation being about 0.04 mg cm^{-2} hr^{-1} (fig. 1). This stability made it easier to interpret the processes occurring during the initial phases of the hot corrosion.

Thermogravimetric Results

A typical hot corrosion curve for IN–738 is shown in figure 3(a), where the specific weight gain is plotted against time. The hot corrosion process for this alloy was characterized by a rather long induction period, that is, a period of little or no weight gain. In fact, the preoxidized specimens initially exhibited a period of slight weight loss, amounting to about 0.7 mg cm^{-2} at about 10 hr. The duration of the so-called induction period is a function of the composition of the alloy, the preoxidation treatment of the specimen, the test temperature, and the amount of Na_2SO_4 applied to induce hot corrosion (ref. 7). Defining the length of the induction period is somewhat arbitrary. In our recent report on the hot corrosion of B–1900 (ref. 1) we defined it as the time when an abrupt change occurs in the slope of the corrosion curve. We will adhere to that definition herein. An examination of figure 3(a) indicates that the induction period was about 55 hr long and the corresponding specific weight gain was 5 mg cm^{-2}. Thus the induction period consisted of a period of small weight loss (up to 10 hr) followed by a long period of moderate weight gain (up to 55 hr).

It is instructive to examine the rate of corrosion during the induction period, after the minimum in the weight gain curve (fig. 3(a)). To this end, we have plotted in figure 4 the specific weight gain, on an expanded scale, against time. The expanded scale is the same scale used in figure 1. It is evident from this plot that the specimen oxidized at a linear rate after about 15 hr, an indication that the oxide formed was not protective in the usual sense. The linear corrosion rate was 0.14 mg cm^{-2} hr^{-1}, about four times the rate of normal oxidation at 24 hr (fig. 1).

The induction period was followed by a period in which the rate of corrosion accelerated rapidly until, at about 60 hr, attack became catastrophic, as shown by the region in which a rapid linear weight gain behavior is displayed. This linear attack continued until about 75 hr, at which time the rate started to decelerate slightly. However, by this time a large fraction of the specimen had been consumed and it was covered with a voluminous, porous, greenish-black oxide. A typical specimen is shown in figure 5. In figure 5(a) the specimen is shown as it appeared on the balance at the end of the 100-hr hot corrosion test. In figure 5(b) it is shown with the oxide removed so that the consumption of the alloy could be apprized. Obviously most of the attack occurred on the bottom half of the specimen. This behavior was found with all of the test specimens. The Na_2SO_4 was very fluid at 975° C and most of it "slumped" to the bottom half of the specimen. The hot corrosion attack occurred primarily on the bottom half and spread very slowly to the upper half of the specimen. This behavior was unlike the hot corrosion of B–1900 and VIA at 900° C described in reference 1, where attack usually began at one or two spots near the middle of the specimen but then spread rapidly over the entire specimen.

Sulfur Dioxide Evolution

The SO_2 evolved during the hot corrosion tests was monitored continuously. Results for a typical specimen are shown in figure 3(b), where the concentration of SO_2 detected in the effluent oxygen is plotted, in parts per million per unit sample area, against the test time. Some SO_2 evolved almost immediately as the sample was brought up to the test temperature. The concentration rose rapidly to about 3.4 ppm cm^{-2} (25 ppm), generally within the first 5 to 10 min. Thereafter the SO_2

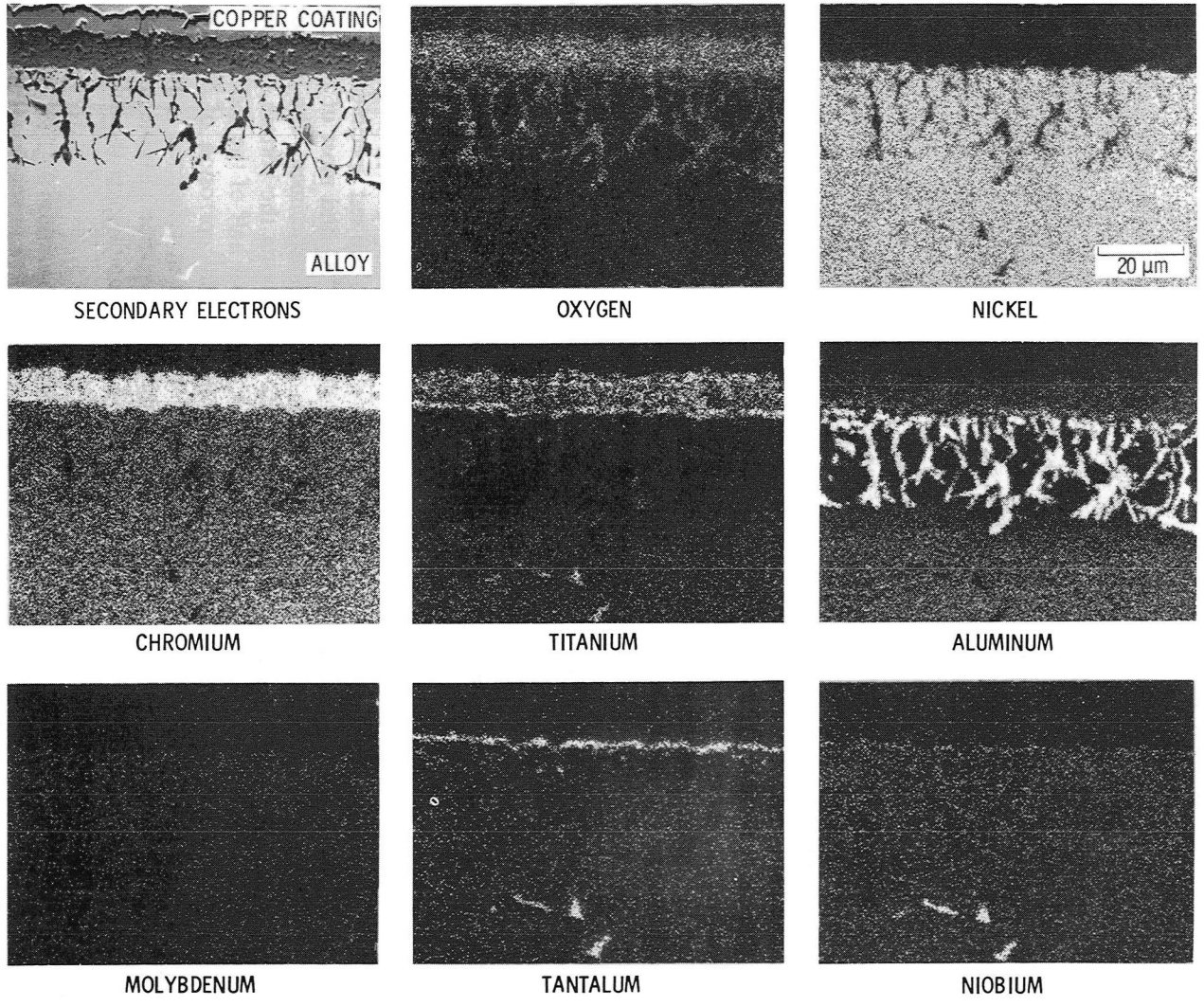

Figure 2.—Secondary electron and X-ray micrographs of IN-738 specimen preoxidized at 975° C for 24 hr in flowing oxygen.

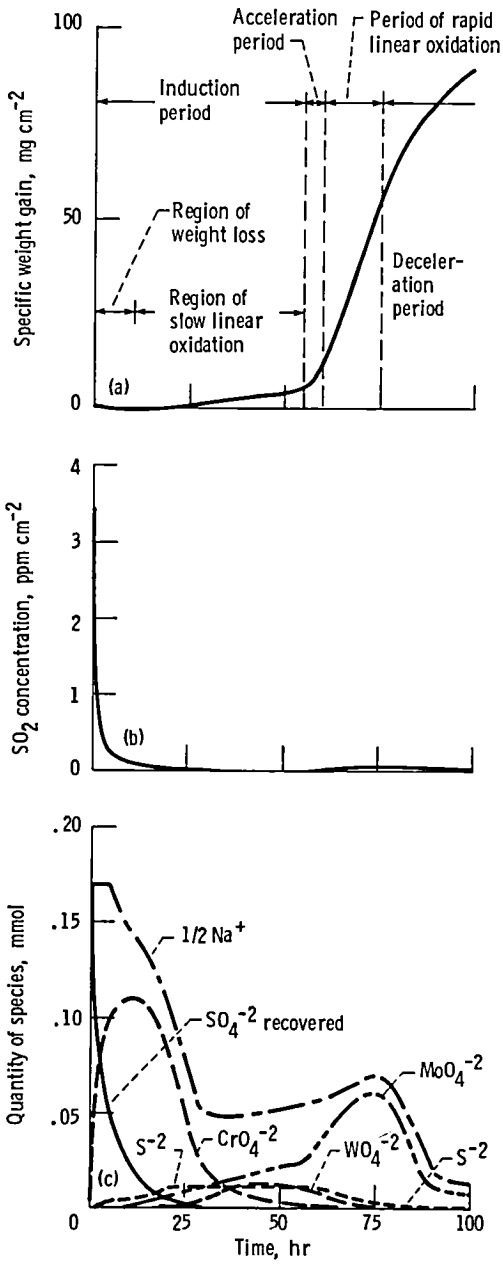

(a) Typical specific weight change.
(b) Concentration of SO_2 evolved.
(c) Quantity of water-soluble species remaining.

Figure 3.—Specific weight change, concentration of SO_2 evolved, and quantity of water-soluble species remaining as a function of time for preoxidized IN-738 corroded at 975° C with 3 mg cm^{-2} Na_2SO_4 in slowly flowing oxygen.

concentration decreased rapidly, reaching about 0.27 ppm cm^{-2} (2 ppm) in 4 hr. It decreased more slowly after that, reaching essentially zero (i.e., <0.02 ppm) at about 20 hr. No further SO_2 above this level was detected until the specimen started corroding catastrophically, at about 57.5 hr. At this time the SO_2 level started to rise slowly, to about 0.014 ppm cm^{-2} (0.1 ppm) by 80 hr, and then

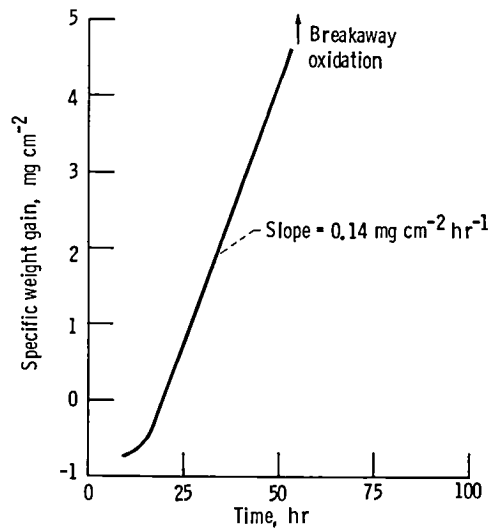

Figure 4.—Replot of weight change data of preoxidized IN-738 presented in figure 3(a) with the scale for the specific weight expanded to the same sensitivity as that of figure 1.

fell back gradually to 0.02 ppm by 110 hr. Although the results for different specimens deviated somewhat from this norm, all exhibited the same qualitative behavior. The greatest variation was in the value of the original peak height, which ranged from 3 to 3.8 ppm cm^{-2} although most specimens were within ±0.25 ppm cm^{-2} of 3.4 ppm cm^{-2}.

Water-Soluble Elements

Specimens were tested for fixed periods of time, and then water-soluble compounds were extracted for chemical analysis. The test times were normalized to a relative time scale by matching the respective individual weight gain with the curve given in figure 3(a). This procedure was necessary because individual specimens varied about ±10 percent in the length of their induction periods. Tests were run for 5 and 15 min, and for 2.5, 5, 10, 15, 20, 30, 40, 50, 56, 60, 73, 83, 90, and 100 hr. The results of chemical analysis are given in figure 3(c), where we have plotted as a function of time the millimols of each element found and the SO_4^{-2} recovered. Individual points have been eliminated for clarity and the data are presented as smoothed curves. The Na_2SO_4 originally applied to the samples is given at zero time and amounted to 0.168 mmol. Because the Na_2SO_4 applied to different samples varied by ±5 percent, all quantities of the soluble species given in figure 3(c) were normalized to 0.168-mmol Na_2SO_4. In addition, the alloy specimens themselves were analyzed for sulfur, and these results are given as sulfides (S^{-2}) in figure 3(c).

The analytical results are different from those obtained in our recent study (ref. 1) of B-1900 and NASA-TRW VIA, alloys for which the protective scale is primarily Al_2O_3. With IN-738 the amount of SO_4^{-2} recovered

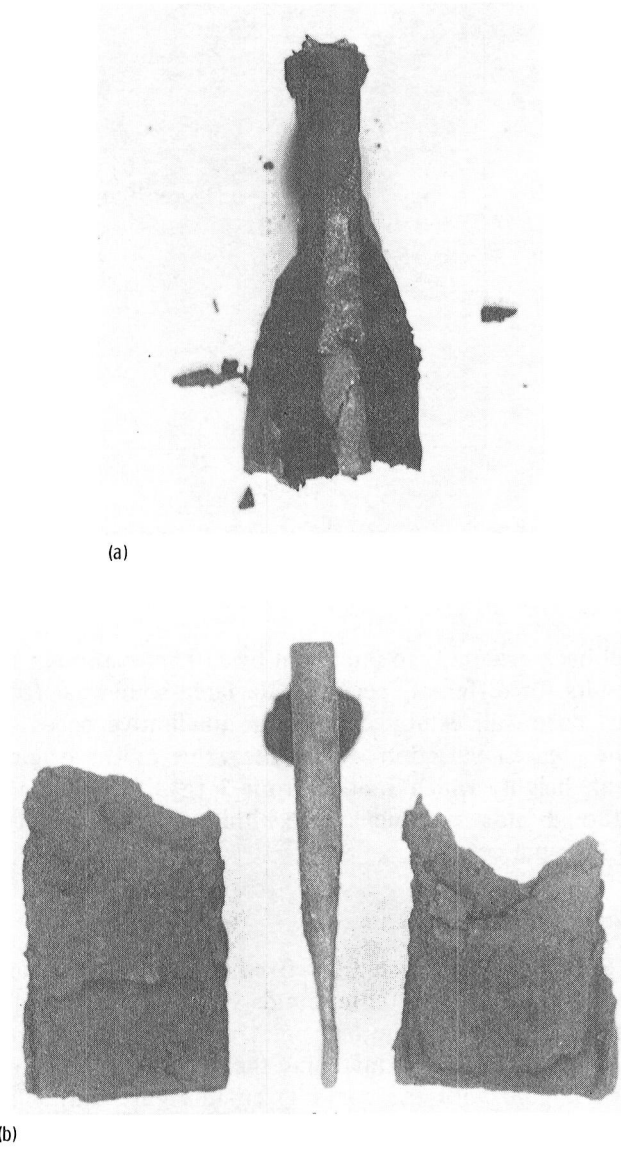

(a) Edge view with oxide scale intact.
(b) Edge view with oxide scale removed.

Figure 5.—Typical IN-738 specimen after corrosion with 3 mg cm^{-2} Na_2SO_4 for 100 hr at 975° C in slowly flowing oxygen.

dropped rapidly from zero time, to 10 percent of its original value in 12.5 hr. It continued to decrease slowly after that, to essentially zero after 25 hr. All of the applied sodium (1/2 Na^+) was completely recovered up to about 5 hr. After that it decreased rapidly, to about 30 percent of its original value at 30 hr. This level persisted until about 40 hr, when it began to rise slightly. It peaked at about 75 hr at 0.07 mmol, then fell sharply to about 0.02 mmol at 90 hr, and finally leveled out at a little over 0.01 mmol at longer times.

The most striking feature of the analytical results was the large quantity of soluble chromium (CrO_4^{-2}) formed: namely, 0.11 mmol. Only 0.03 mmol was found in similar studies with B-1900 and VIA (ref. 1). The soluble chromium was evidenced by the yellow chromate color found on the surfaces of cooled samples and also by the yellow color of the water-wash solutions extracted for analysis. The quantity of soluble chromium rose rapidly from the beginning of the test, maximized at around 10 hr, and then fell in a rapid, nearly linear manner until about 30 hr. After that it decreased slowly and reached very small values after about 60 hr.

Soluble molybdenum[1] (MoO_4^{-2}) appeared early in the hot corrosion process, after about 10 hr. It increased linearly throughout the long induction period, to more than 0.02 mmol at 55 hr. It increased more rapidly during the catastrophic corrosion of the sample (55 to 75 hr) and maximized at 0.06 mmol at 75 hr. It then decreased rapidly over the next 15 hr, back to about 0.01 mmol. Soluble tungsten (WO_4^{-2}) was detected at about the same time as soluble molybdenum, at 10 hr. However, it increased more slowly than molybdenum and maximized earlier, namely, 0.012 mmol at 40 hr.

All extracted solutions were also analyzed for soluble aluminum, titanium, tantalum, niobium, and nickel in addition to the species discussed above. The occurrence of soluble aluminum is an important feature in the hot corrosion of B-1900 and VIA (ref. 1), but none could be detected in any of the samples from IN-738. Of these five elements, only soluble nickel was found and this at levels less than 0.01 mmol. It occurred during the period of catastrophic corrosion and decreased after 80 hr.

Sulfur was found in the 5- and 10-hr alloy specimens at a level of 0.004 mmol. The value rose to 0.01 mmol in the 20-hr specimen and remained constant at that level until after 60 hr, at which time it began decreasing, reaching zero at 100 hr.

It is informative to compare the loss of sulfate with the cumulative quantity of SO_2 evolved during the course of hot corrosion. If the loss of sulfate is due to reaction with the oxides in the scale, namely Cr_2O_3 and TiO_2, there should have been a direct proportionality between the cumulative SO_2 evolved and the sulfate reacted, as shown by the equations

$$Cr_2O_3 + 2Na_2SO_4(l) + 1/2\ O_2 \rightarrow 2Na_2CrO_4(l) + 2SO_2 \quad (1)$$

$$n\ TiO_2 + Na_2SO_4(l) \rightarrow Na_2O(TiO_2)_nSO_2 + 1/2\ O_2 \quad (2)$$

Cumulative values for the SO_2 evolved were obtained by numerically integrating the monitored concentrations over time. These values are compared with the amount of

[1]Soluble molybdenum was considered to come from Na_2MoO_4 even though MoO_3 is slightly soluble in hot water. The assumption is probably valid because of the greater solubility of Na_2MoO_4 and, more importantly, its great thermodynamic stability.

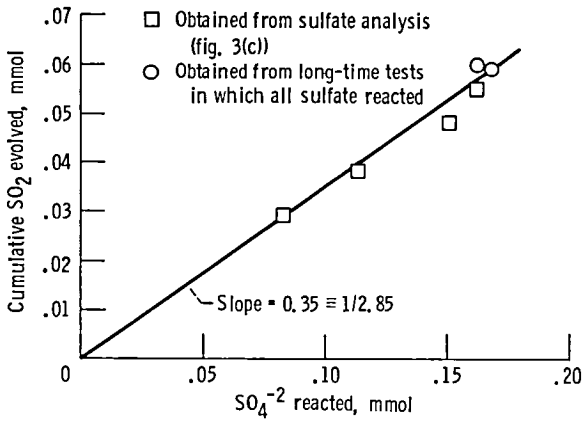

Figure 6.—Relationship between cumulative quantity of SO_2 evolved and quantity of sulfate reacted during hot corrosion of IN-738 at 975° C.

sulfate reacted in figure 6, where all quantities are expressed in millimols. The amount of sulfate reacted was obtained in two ways. The square points were obtained from the curve of the sulfate analysis given in figure 3(c). The circular points were obtained from long-time tests in which all of the sulfate applied reacted. Using the weight of the sulfate applied was probably more accurate than using the sulfate analysis.

It was evident that a direct relationship existed between the amount of SO_2 evolved and the sulfate reacted. However, it was also evident that it was not a one-to-one relationship as one would expect for reaction (1) or (2): the millimols of SO_2 evolved were only about 0.35 of the millimols of sulfate reacted. The discrepancy arose from the fact that we did not take into account the SO_3/SO_2 thermodynamic equilibrium in our calculations: actually, both SO_3 and SO_2 were present in the effluent gas. As shown in reference 1, the SO_3/SO_2 equilibrium was characteristic not of the furnace temperature,[2] but of some lower temperature. Because the effluent gas seemed to be quenched at the bottom of the furnace, accurate theoretical correction for the presence of SO_3 was precluded. However, this difficulty did not detract from the direct relationship found between the SO_2 evolved and the sulfate reacted and lent credence to the occurrence of reaction (1) or (2) in the early part of the hot corrosion process.

Microprobe Analysis

Samples were prepared for microprobe examination from specimens that had been tested for 5 min and 5, 10, 20, 30, 40, 48, 56, 62, 68, 77, and 90 hr. All of the samples were examined carefully in several different areas, although primarily in the bottom half of the specimens, where the hot corrosion occurred. For the sake of brevity only micrographs of the most pertinent areas are presented. The 5-min sample served as a point of reference for the specimens corroded for longer times and more importantly proved the efficacy of our sample preparation techniques. The secondary electron and elemental X-ray micrographs for this sample are presented in figure 7. The area displayed was just below the middle of the specimen and shows the upper part of the Na_2SO_4 deposit that had slumped onto the bottom half of the specimen. The micrographs show that the oxide layer had been little affected by the Na_2SO_4 in this short time and that the scale was essentially the same as that of the preoxidized sample shown in figure 2.

The micrographs for the 5-hr sample, shown in figure 8, were radically different. The original, continuous Cr_2O_3–TiO_2 layer had been largely removed, as shown by islands of the alloy, with most of the active elements leached out, protruding along the surface. Only molybdenum and tungsten seemed to be present in the alloy islands along with the nickel and cobalt. The outer oxide layer was thus no longer continuous but still seemed to be composed primarily of Cr_2O_3 and TiO_2. The depletion of chromium in the alloy was becoming more pronounced. Although sulfur was not evident in these micrographs, sodium lay along the upper edge of the sample and seemed to be associated with chromium or titanium. The micrographic observations of this sample were complicated by the effects of a void that encircled most of the sample cross section between the oxide layer and the copper coating. Such voids occurred on both the 5-and 10-hr samples and also on duplicate samples taken at these times. A large drop of Na_2CrO_4 was observed visually on these specimens after hot corrosion testing, and it is believed that the void developed during polishing by removal of this Na_2CrO_4. In the microprobe examination X-rays emanating from the void complicated the interpretation of some of the elemental X-ray micrographs, especially those for chromium and sodium. The chromium micrograph in figure 8 indicates the presence of chromium in the void and depicts an almost continuous Cr_2O_3 layer on the sample even though the secondary electron micrograph clearly shows that the Cr_2O_3 layer was partly noncontinuous. Of course, the problem resulted from the poorer resolution inherent in the X-ray micrographs as compared with secondary and backscattered electron micrographs. Light micrographs were not affected by the presence of the void and show more unambiguously that the original continuous Cr_2O_3/TiO_2 layer had been removed and replaced by a discontinuous oxide. Light micrographs of the 5-hr sample and the original preoxidized sample are presented in figure 9 for comparison. The micrographs of the 10-hr sample were similar to those of the 5-hr sample and thus were omitted herein.

[2]The SO_3/SO_2 ratio in ref. 1 was mistakenly inverted during printing to SO_2/SO_3. It should be $SO_3/SO_2 = 0.32$ at 900° C.

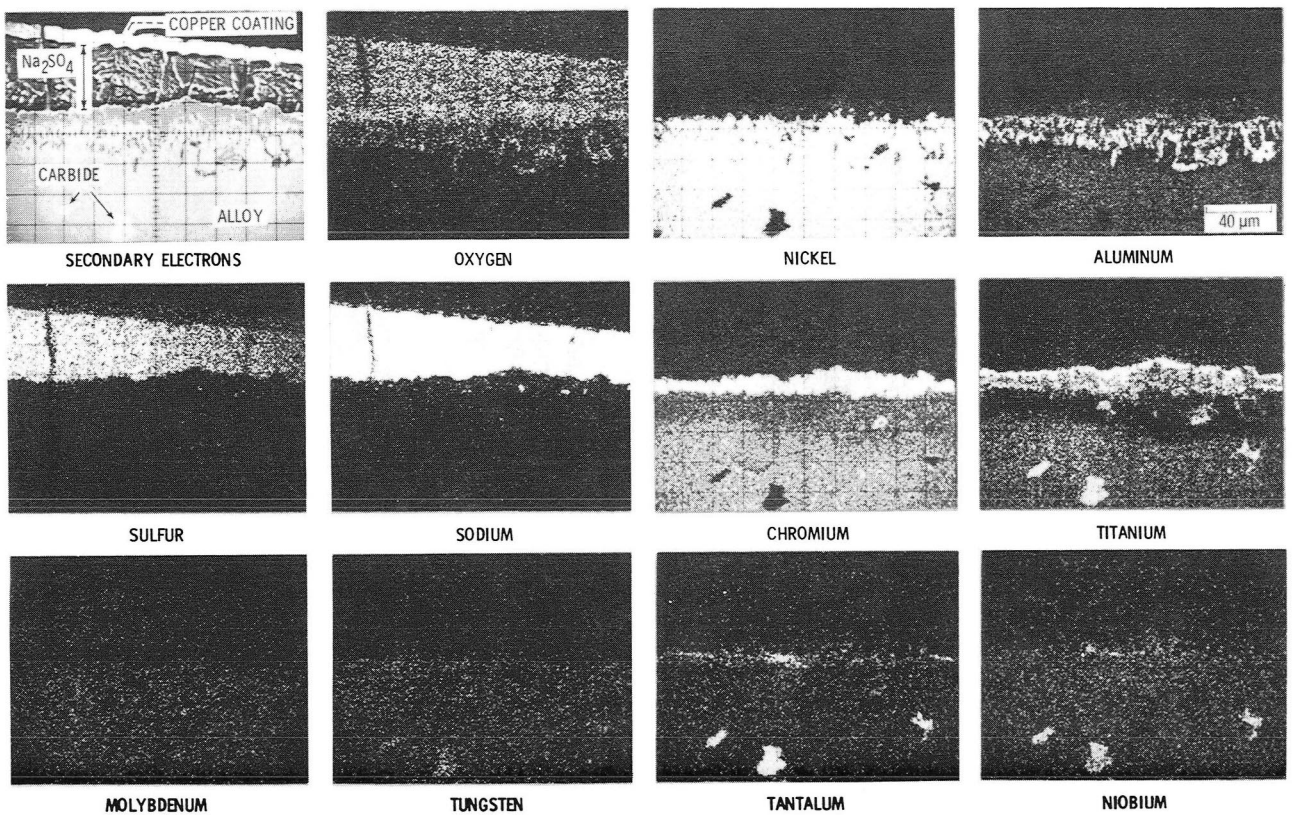

Figure 7.—Secondary electron and X-ray micrographs of preoxidized IN-738 specimen corroded for 5 min at 975° C with 3 mg cm^{-2} Na_2SO_4.

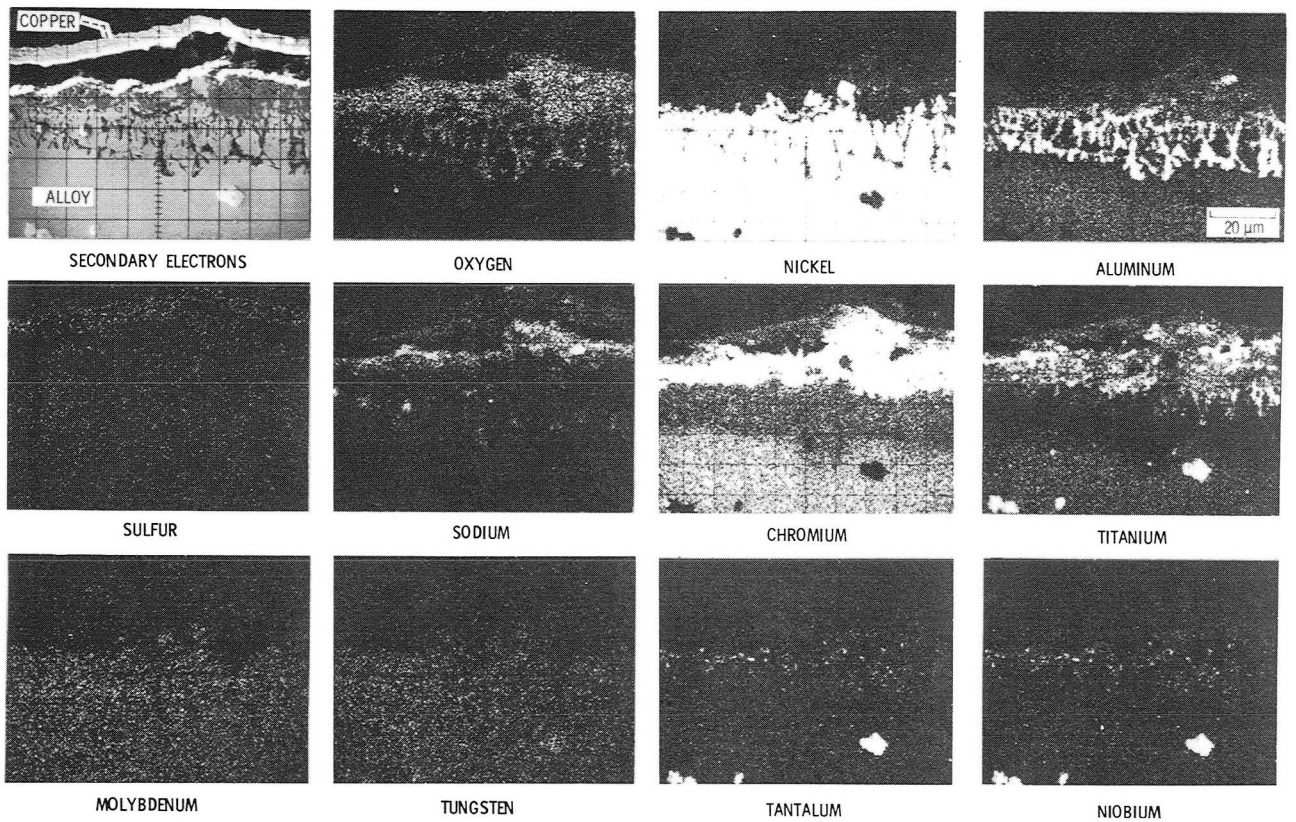

Figure 8.—Secondary electron and X-ray micrographs of preoxidized IN–738 specimen corroded for 5 hr at 975° C with 3 mg cm^{-2} Na_2SO_4.

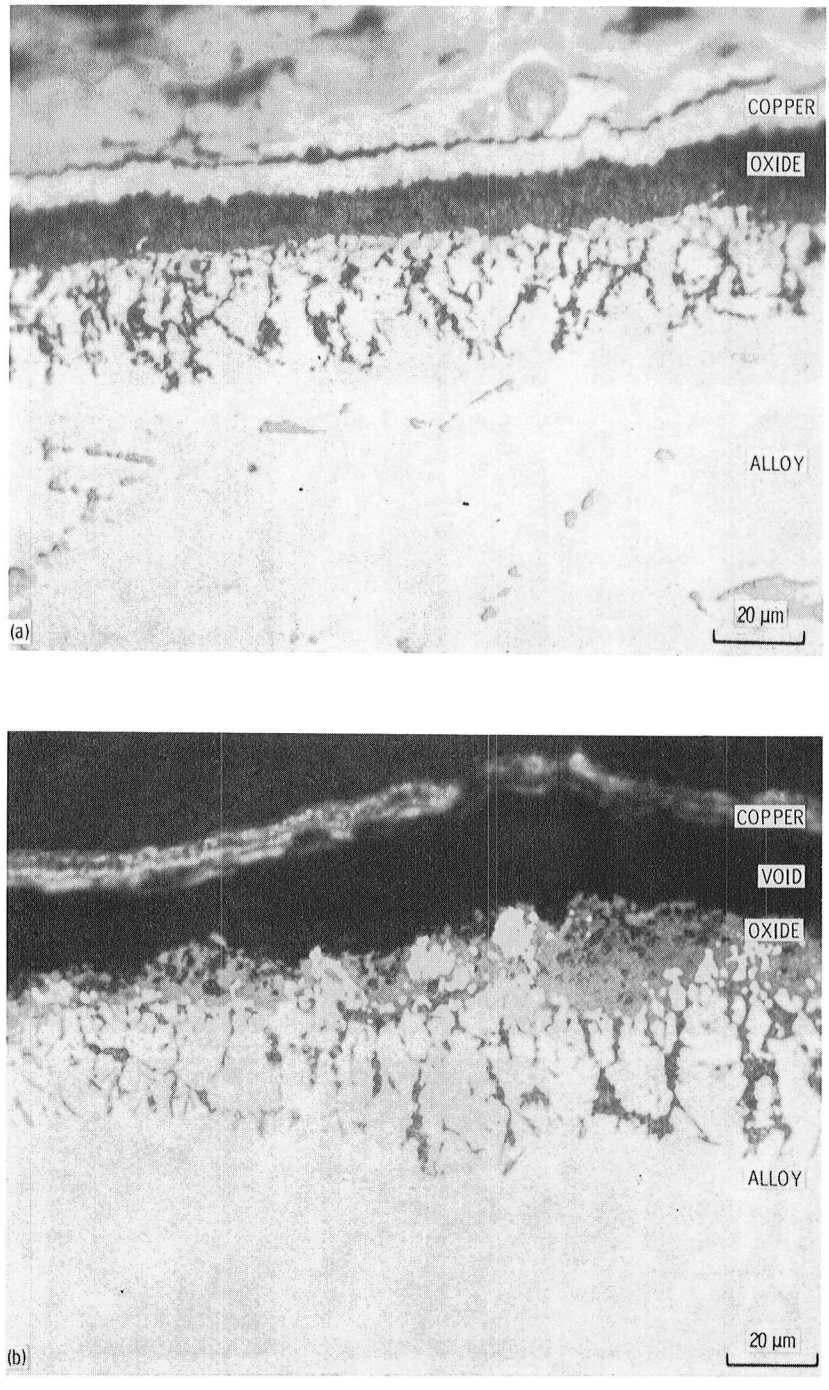

(a) Preoxidized for 24 hr at 975° C.
(b) Preoxidized for 24 hr and corroded for 5 hr at 975° C with 3 mg cm^{-2} Na_2SO_4.

Figure 9.—Light micrographs of IN-738 specimens.

For the 20-hr sample the micrographs (fig. 10) show that the oxide scale was reforming, having increased to 20 to 30 μm in thickness. The oxide was advancing into the region where the Al_2O_3 tentacles existed and was still primarily Cr_2O_3 and TiO_2 though some NiO was now scattered throughout. Of course, the engulfed Al_2O_3 was also in the scale. The depletion zone for chromium was much wider and more depleted, as was that for titanium. Near the bottom of the depletion zone chromium sulfides are evident, and other sulfides, probably of chromium, were scattered throughout the upper portion of the depletion zone. Sodium was still situated along the outer edge of the sample and was probably associated with chromium and titanium. Some areas of sodium within the scale (i.e., the bright areas in the secondary electron micrograph) were associated with tantalum or niobium and were probably $NaTaO_3$ or $NaNbO_3$, formed from carbides that were there originally. Some of the sodium was also associated with the tantalum and niobium oxides lying along the bottom edge of the scale. No oxides of molybdenum or tungsten were evident; these components still seemed to be associated with the leached Ni-Co islands that were isolated between the Al_2O_3 tentacles in the growing scale: see nickel micrograph in figure 10.

The micrographs of the 30-hr sample (fig. 11) show that the oxide scale had continued to grow, being 25 to 35 μm thick. It was composed of Cr_2O_3, TiO_2, engulfed Al_2O_3, and NiO. "Ghosts" of the Al_2O_3 tentacles appear near the bottom of the scale: the dark stringers in the backscattered electron micrograph. The nickel oxide was becoming more prominent and some was concentrated along the outer edge of the oxide layer. Sodium was still distributed throughout the scale and in oxidized carbides with tantalum and niobium: one very prominent $NaTaO_3$-$NaNbO_3$ area was located in the upper central section of the oxide scale. Sulfur was at the bottom of the depletion zone and down along a grain boundary and was associated primarily with titanium. The most important feature on this sample was the appearance of an area of MoO_3-WO_3 at the bottom of the scale near the left side: the light gray area about 5μm in diameter in the backscattered electron micrograph. This was the first appearance of molybdenum and tungsten oxides.

In the 40-hr sample the oxide was about 30 to 35 μm thick although in a few spots it had grown to a thickness of 60 μm. One such area is shown in figure 12. The leached Ni-Co islands, which were isolated by the Al_2O_3 tentacles, seemed to have oxidized. The ghosts of the tentacles appear as the darker stringers in the backscattered electron micrograph, and they are still present in the aluminum micrograph. At the lower edge of the oxidized islands were isolated areas of MoO_3-WO_3. They are the bright areas in the backscattered electron micrograph, and they appear in the molybdenum and tungsten micrographs but with poorer resolution. They must have originated from the molybdenum and tungsten that were still in solution in the Ni-Co islands. The composition of the scale was similar to that of the 30-hr sample. However, all of the sodium in this area seemed to be tied up as $NaTaO_3/NaNbO_3$, and little or no sulfur was in evidence.

In the 48-hr sample a large fraction of the oxide was 60 μm thick, and as shown in figure 13, the morphology of these areas was similar to that of the thick area of the 40-hr sample. The backscattered electron micrograph shows the oxidized Ni-Co islands, lighter gray, with the ghosts of the Al_2O_3 tentacles still observable as darker gray tentacles. Bright areas of MoO_3-WO_3 lay along the bottom edge of the scale. The MoO_3-WO_3 areas were still discrete, but they were so numerous as to be almost continuous. Although some sodium was combined with the tantalum and niobium, some was also associated with the MoO_3-WO_3 areas, most probably as Na_2MoO_4 or Na_2WO_4. Sulfur was not very prevalent but occured in a very faint concentration in the MoO_3-WO_3 areas. In addition to the NiO observed in the oxidized islands, some was also apparent along the outer edge of the scale.

In the 56-hr sample most of the oxide layer was similar to the area of the 48-hr sample presented in figure 13. However, in two areas the discrete MoO_3-WO_3 areas had obviously merged to form a large molten phase probably composed of MoO_3-WO_3 and Na_2MoO_4-Na_2WO_4. Micrographs of one of these areas are shown in figure 14. The light area along the bottom of the oxide scale in the backscattered electron micrograph is the molten MoO_3-WO_3/Na_2MoO_4-Na_2WO_4 phase. The sulfides had been engulfed by the molten phase and sulfur appeared in it. Sodium was distributed throughout the entire oxide layer and also appeared in the molten phase. The oxide scale was 80 to 90 μm thick and was composed of all of the metallic components of the alloy except molybdenum and tungsten. The striated or layered structure displayed here is characteristic of that found when acidic fluxing is occurring (ref. 1, fig. 14).

The 62-, 68-, and 77-hr samples all showed increasing occurrence of areas similar to that described for the 56-hr sample (fig. 14). One such area from the 77-hr sample is shown in figure 15. Again we see the large molten phase of MoO_3-WO_3/Na_2MoO_4-Na_2WO_4 lying along the underside of the oxide layer. The internal sulfides had been engulfed as the molten phase progressed across the sample under the scale. Again, the oxide was striated, or layered, and consisted of oxides of all of the metals in the alloy except molybdenum and tungsten.

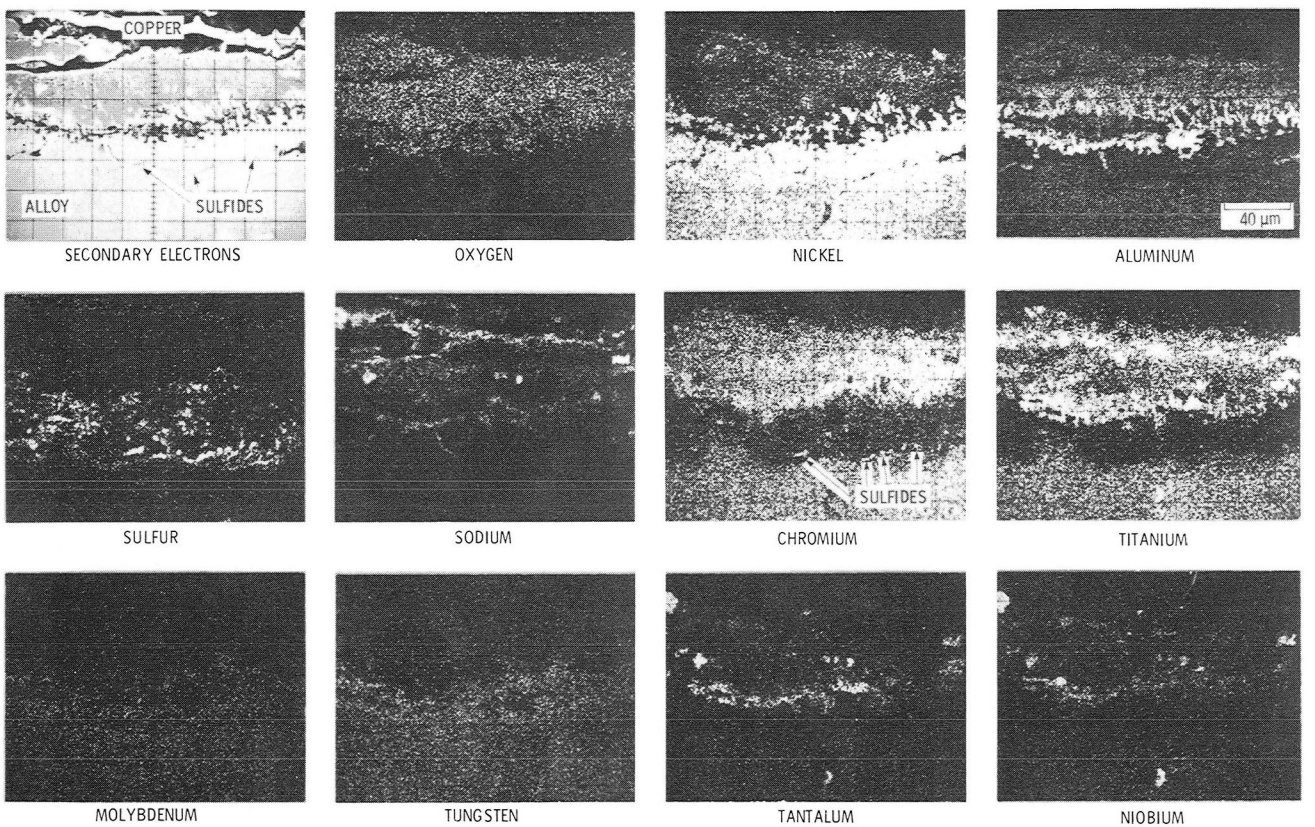

Figure 10.—Secondary electron and X-ray micrographs of preoxidized IN-738 specimen corroded for 20 hr at 975° C with 3 mg cm^{-2} Na_2SO_4.

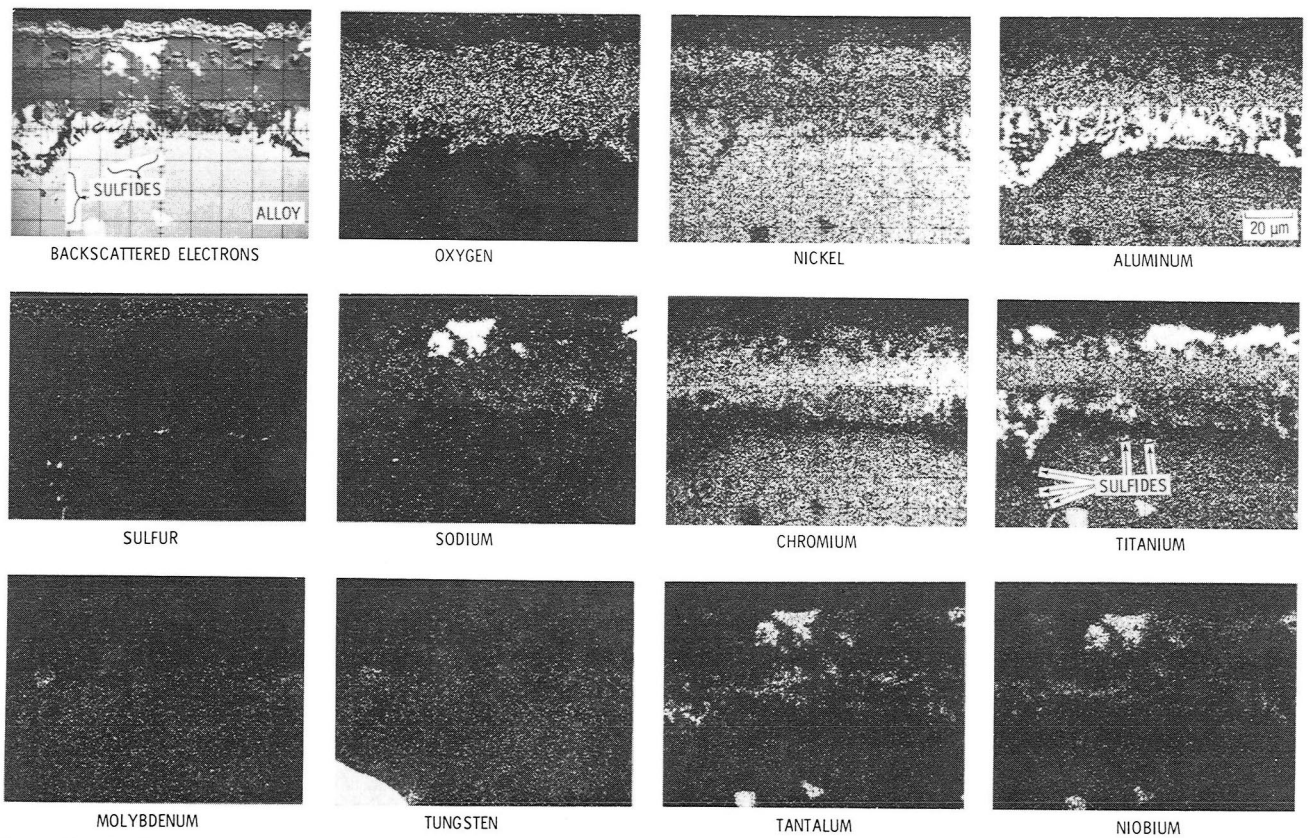

Figure 11.—Backscattered electron and X-ray micrographs of preoxidized IN-738 specimen corroded for 30 hr at 975° C with 3 mg cm^{-2} Na_2SO_4.

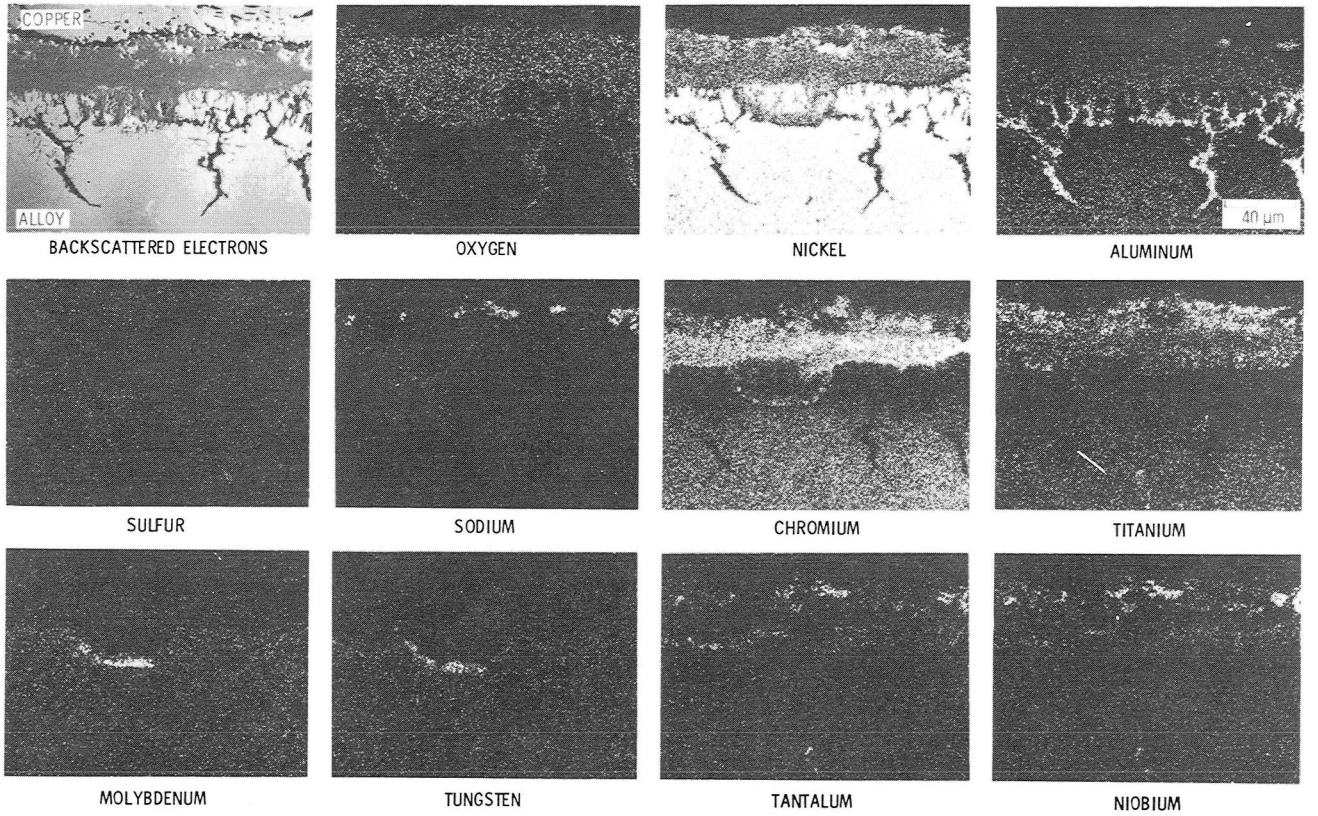

Figure 12.—Backscattered electron and X-ray micrographs of preoxidized IN-738 specimen corroded for 40 hr at 975° C with 3 mg cm^{-2} Na_2SO_4.

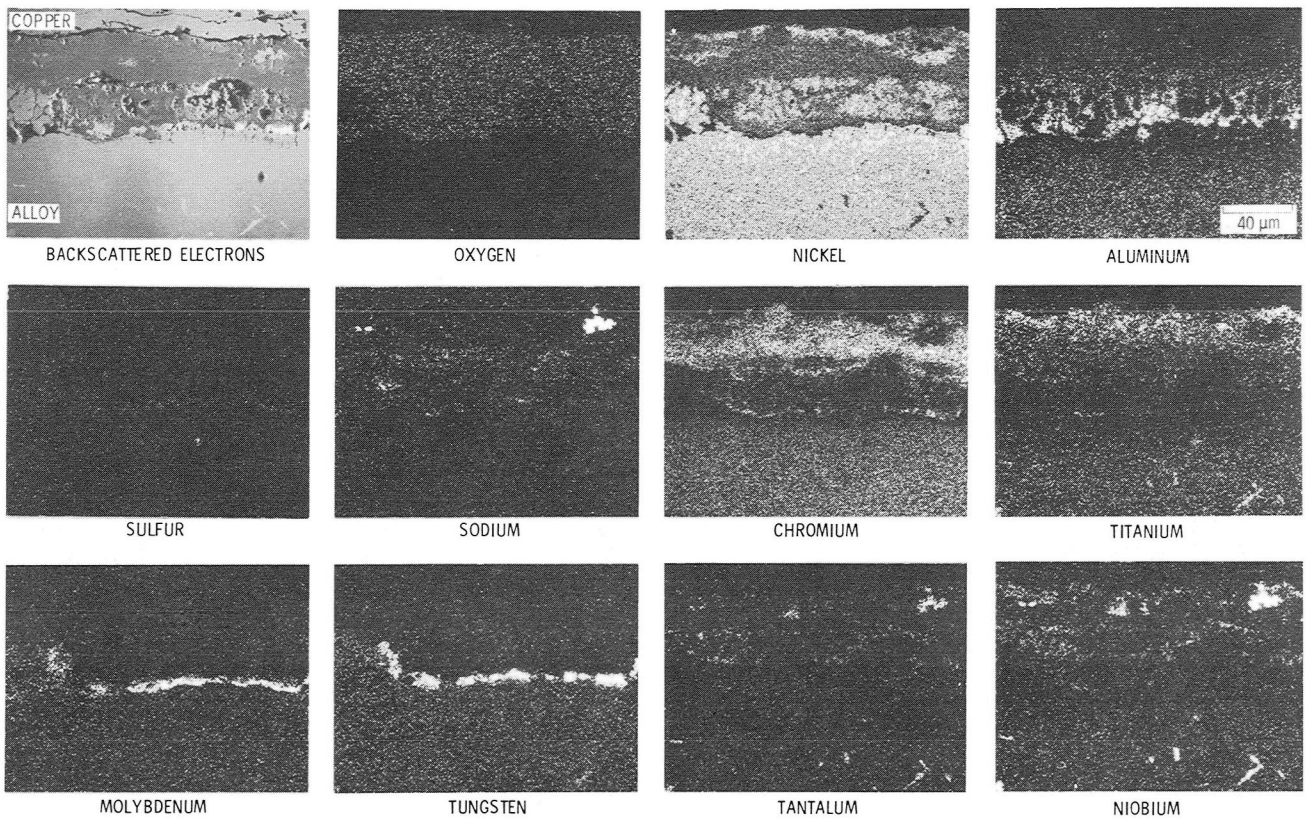

Figure 13.—Backscattered electron and X-ray micrographs of preoxidized IN-738 specimen corroded for 48 hr at 975° C with 3 mg cm^{-2} Na_2SO_4.

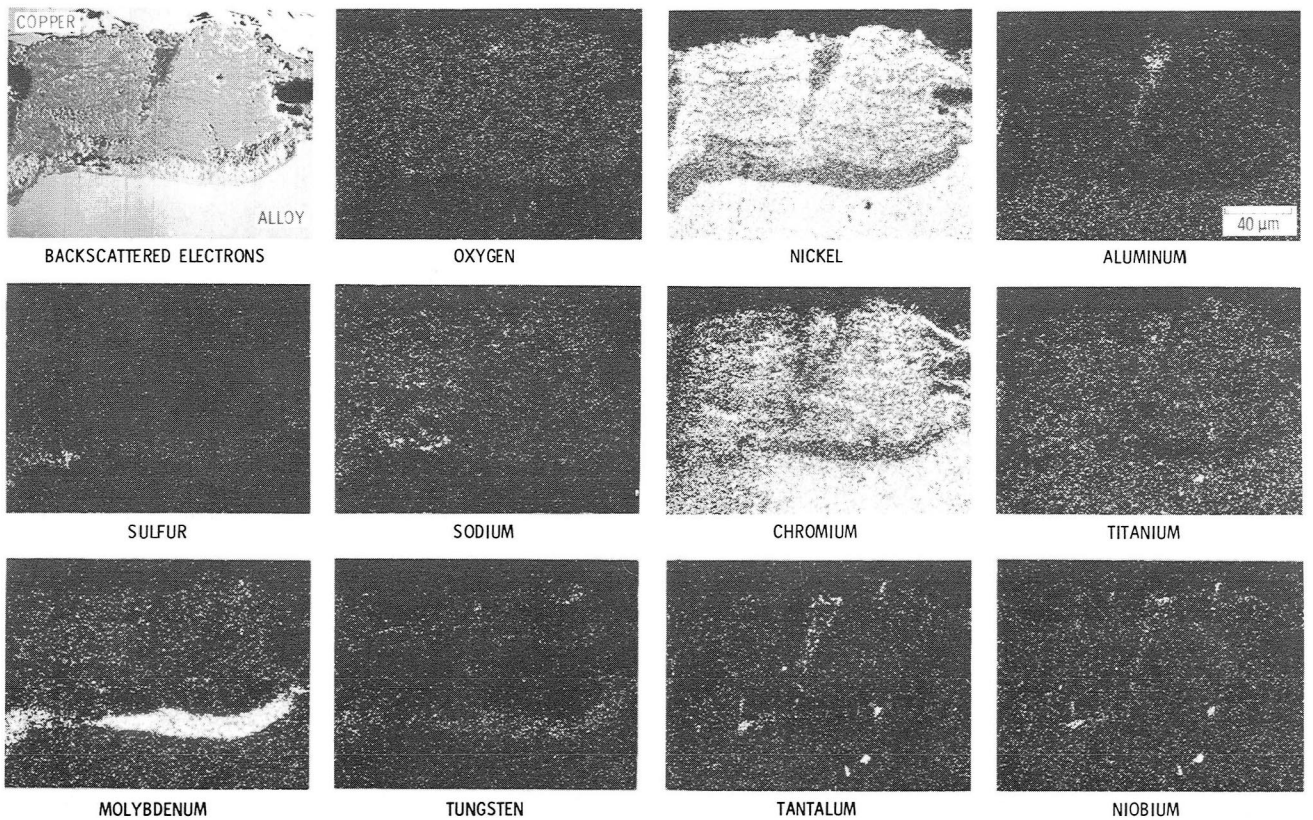

Figure 14.—Backscattered electron and X-ray micrographs of preoxidized IN-738 specimen corroded for 56 hr at 975° C with 3 mg cm^{-2} Na_2SO_4.

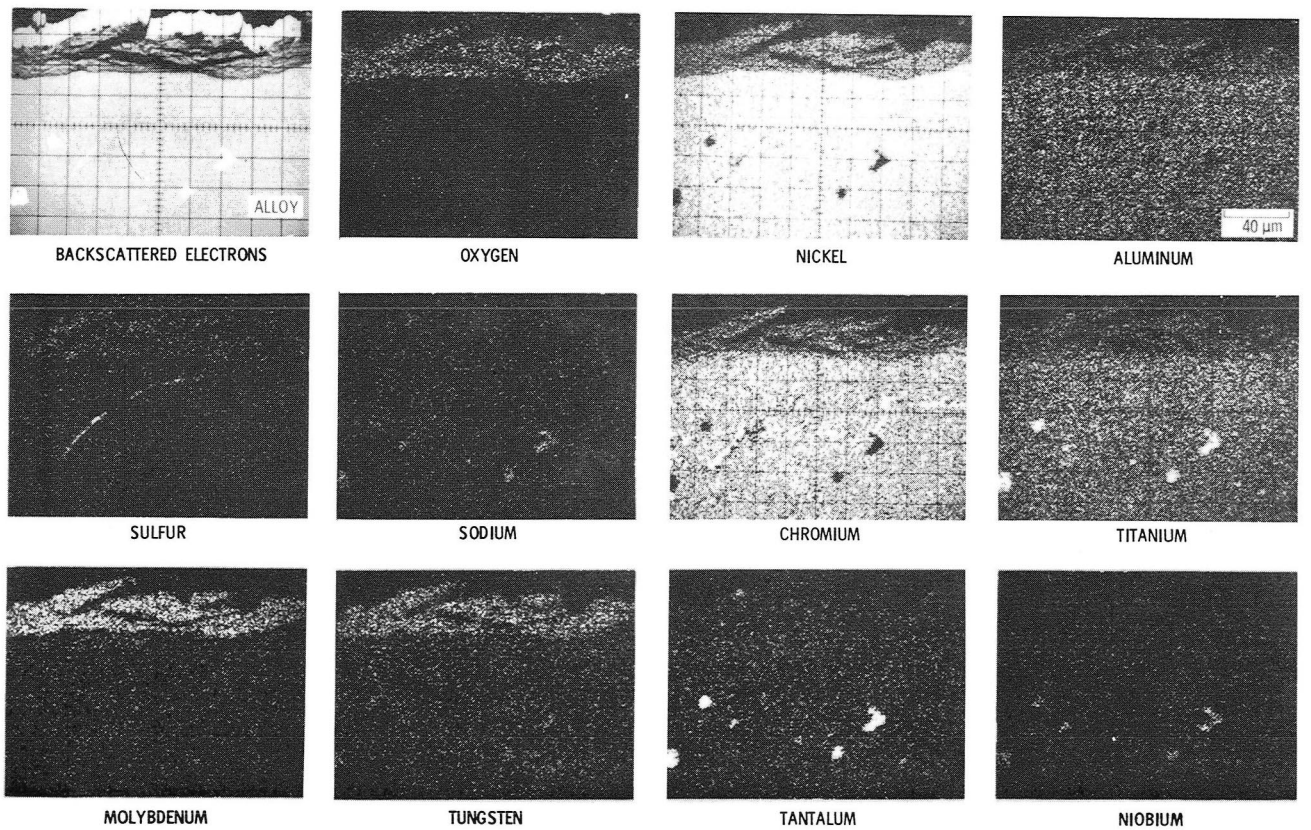

Figure 15.—Backscattered electron and X-ray micrographs of preoxidized IN-738 specimen corroded for 77 hr at 975° C with 3 mg cm^{-2} Na_2SO_4.

In the 90-hr sample the molten phase under the scale had decreased in prominence. In some areas the molten MoO_3-WO_3/Na_2MoO_4-Na_2WO_4 has been converted to solid $NiMoO_4$-$NiWO_4$.[3] One such area is shown in figure 16. Here most of the thick oxide scale had peeled off the sample, leaving just the $NiMoO_4$-$NiWO_4$ layer. The layer exhibited a great deal of cracking within itself, which resulted from the $NiMoO_4$ undergoing an allotropic transformation upon cooling. Some titanium, aluminum, and chromium were associated with the cracked layer, and even a little sulfur was discernible in it. Sulfur was primarily concentrated along a deep grain boundary. Sodium was no longer observed with the molybdate but had diffused deep into the alloy, where it had combined with tantalum and niobium located in internal carbides.

Rate Determinations of Pertinent Processes

To properly interpret the results presented so far, it seemed apparent that measurements of the rate of several pertinent physical and chemical processes were required. Extensive investigation of these processes was beyond the scope of this work. In addition, for the results to be applicable, we were constrained by the confines of our experimental apparatus. Nevertheless the work performed was sufficient to allow the formulation of some reasonable conclusions.

Evaporation rate of Na_2SO_4 and Na_2CrO_4.—Deposits of 3 mg cm^{-2} of Na_2SO_4 or Na_2CrO_4 were air brushed onto coupons of the same size as the oxidation specimens. Gold coupons were used for Na_2SO_4 (ref. 16) and platinum for Na_2CrO_4. The weight loss was determined with the Cahn microbalance under the same experimental conditions as were used in the hot corrosion tests: namely, oxygen flow of 620 milliliters min^{-1} and temperature of 975° C. Weight losses were monitored for periods up to 100 hr and were linear in time. After the tests the cooled coupons were water washed and the resulting solutions analyzed for sodium and SO_4^{-2} or CrO_4^{-2}. In all cases the analyses checked well with the measured weight losses. In addition, the pH values of the wash solutions were measured and were found to check well with the pH values of prepared solutions of the respective salts. This agreement in pH values indicated that no dissociative vaporization occurred.[4] After-experiment weights of the coupons were the same as the before-experiment weights, showing that the coupons and the salts did not react. The rates of evaporation determined for the two salts are given in table II. We see that Na_2CrO_4 evaporated about 1.5 times more rapidly than Na_2SO_4.

Rate of reaction of Na_2SO_4 with the pure oxides Cr_2O_3 and TiO_2.—The two reactions studied can be written

$$Cr_2O_3 + 2Na_2SO_4(l) + 3/2\,O_2 \rightarrow 2Na_2CrO_4(l) + 2SO_3(g) \quad (3)$$

$$n\,TiO_2 + Na_2SO_4(l) \rightarrow Na_2O(TiO_2)_n + SO_3(g) \quad (4)$$

The same techniques employed in the hot corrosion tests of IN-738 were used here, except that the flow rate used was 1250 milliliters min^{-1} instead of 620 milliliters min^{-1}. The increased flow was necessitated because of a leak in the water permeation dryer of the SO_2 detector. This change had no apparent effect on the kinetic results. The Cr_2O_3 sample was made by preoxidizing a coupon of pure chromium at 975° C. Oxidation was continued until the scale contained about three times the amount of Cr_2O_3 required for reaction with the Na_2SO_4 to be applied. The TiO_2 sample was made by plasma spraying high-purity TiO_2 onto a platinum coupon and annealing at 975° C for 2 hr. Here also, the TiO_2 applied was more than required for reaction with Na_2SO_4.

The results for one of the Cr_2O_3 specimens, which was tested for 2.5 hr, are shown in figure 17. We have plotted as a function of time the specific weight gain and the concentration of SO_2 evolved in parts per million per unit area of the specimen. The specific weight underwent a small initial increase followed by a loss during the period that the $SO_2 + SO_3$ was volatilizing rapidly. Finally a slow increase occurred as some further oxidation of the chromium coupon ensued. The concentration of SO_2 evolved rose rapidly to 4.3 ppm cm^{-2} and then fell at a fast, though decreasing, rate. At the end of the experiment it was only 0.2 ppm cm^{-2}. As shown in figure 6, the quantity of SO_2 evolved was proportional to the amount of SO_4^{-2} reacted. As a corollary to this, it can be concluded that the amount of SO_2 evolving at any time was proportional to the rate of reaction of the SO_4^{-2} at that time. Because the amount of SO_2 evolving determines its concentration in the gas phase, the concentration of SO_2 is then proportional to the rate of reaction of the SO_4^{-2}. Thus the low value for the concentration of SO_2 at the end of the experiment indicated that the reaction between Cr_2O_3 and Na_2SO_4 had been mostly completed. This conclusion was supported by the chemical analyses of the water-wash solutions, the results of which are given in the first line of table III. They show that only 0.00385 mmol of SO_4^{-2}

[3]The $NiMoO_4$-$NiWO_4$ was identified by X-ray diffraction analysis of the surface of companion specimens.

[4]Some SO_2 was detected during the Na_2SO_4 evaporation: being 0.026 ppm cm^{-2} (0.18 ppm) at the beginning of the test and 0.016 ppm cm^{-2} (0.11 ppm) after 100 hr. This SO_2 probably originated not from dissociative vaporization of Na_2SO_4 but from reaction between the vaporizing Na_2SO_4 and the hot quartz furnace tube: $SiO_2 + Na_2SO_4 \rightarrow Na_2SiO_3 + SO_3(g)$.

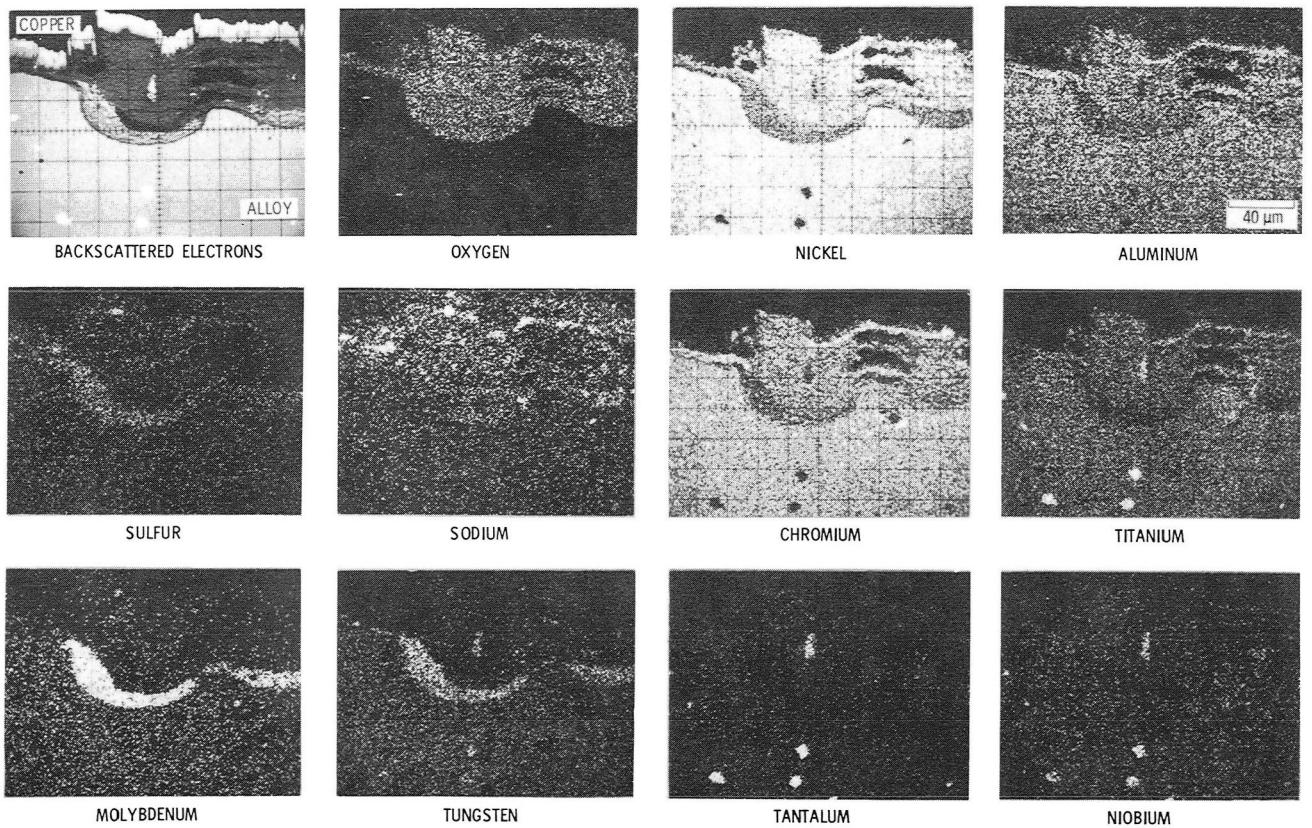

Figure 16.—Backscattered electron and X-ray micrographs of preoxidized IN-738 specimen corroded for 90 hr at 975° C with 3 mg cm^{-2} Na_2SO_4.

TABLE II.—RATES OF PERTINENT PROCESSES

System	Evaporation rate, mmol cm^{-2} hr^{-1}	First-order rate constant, k_1		Zero-order rate constant, k_0	
		hr^{-1}	min^{-1}	mmol $cm^{-2}hr^{-1}$	mmol $cm^{-2}min^{-1}$
$Na_2SO_4(l) \rightarrow Na_2SO_4(g)$	1.0×10^{-4}	---	---	---	---
$Na_2CrO_4(l) \rightarrow Na_2CrO_4(g)$	1.5×10^{-4}	---	---	---	---
$Cr_2O_3 + 2Na_2SO_4(l) + 3/2O_2 \rightarrow 2Na_2CrO_4(l) + 2SO_3(g)$	---	1.55	2.6×10^{-2}	---	---
$nTiO_2 + Na_2SO_4(l) \rightarrow Na_2O(TiO_2)_n + SO_3(g)$	---	---	---	1.25×10^{-3}	2.1×10^{-5}
$nTiO_2 + Na_2CrO_4(l) \rightarrow Na_2O(TiO_2)_n + CrO_3(g)$	---	---	---	5.9×10^{-4}	9.8×10^{-6}

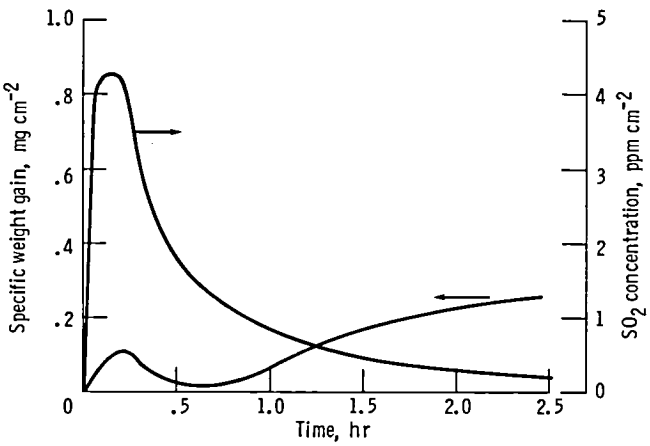

Figure 17.—Specific weight gain and concentration of SO_2 evolved as a function of time for preoxidized chromium specimen corroded at 975° C in flowing oxygen with 3 mg cm^{-2} Na_2SO_4. (Sample area, 2.9 cm^2.)

was recovered from the specimen at the end of the experiment (column 4), as compared with 0.0656 mmol applied (column 3). Thus 94 percent (column 6) of the SO_4^{-2} reacted in the 2.5-hr period of the experiment. The millimols of CrO_4^{-2} formed should equal the millimols of SO_4^{-2} reacted (see reaction (3)), in this case 0.0617 mmol. The amount of CrO_4^{-2} found by analysis was almost identical to this (column 7). In table III we have also given in column 8 the total millimols of SO_2 evolved, which was obtained by integrating under the SO_2 curve of figure 17. Comparing this with the millimols of SO_4^{-2} that reacted, in column 9, shows that the ratio, 0.40, was somewhat larger than that obtained in figure 6, 0.35.

Another specimen of oxidized chromium was hot corroded for a much longer time, 120 hr, to see if chromium would corrode catastrophically. No such corrosion was observed; in fact, the specimen slowly lost weight throughout the 120 hr. The results are summarized in the second line of table III. All of the SO_4^{-2} reacted (columns 4 and 6) but no CrO_4^{-2} (column 7) was found in the wash solution (no Na^+ was found either).

Calculations of the rate of evaporation of Na_2CrO_4, based on the results given in the last section, indicated that all of the Na_2CrO_4 formed from the amount of Na_2SO_4 reacted should have evaporated in 120 hr, just the length of the test. In column 8 we see that the ratio of the total amount of SO_2 evolved to the amount of SO_4^{-2} reacted was 0.355, which is close to the value obtained from the IN-738 data presented in figure 6.

We desire to calculate a rate constant for reaction (3) from the data shown in figure 17 (i.e., the concentration of SO_2 as a function of time). As stated above, the concentration of SO_2 should be proportional to the rate of reaction of SO_4^{-2}. Because the SO_2 concentration fell rapidly, we have assumed that the reaction was first order with respect to the concentration of SO_4^{-2}. Therefore the kinetics should be described by the equation

$$-\frac{dC}{dt} = k_1 C \tag{5}$$

where k_1 is the first-order rate constant and C is the concentration of SO_4^{-2} at time t. Integration of this equation yields

$$\log\left(\frac{C_0}{C}\right) = \frac{k_1 t}{2.303} \tag{6}$$

where C_0 is the initial concentration of SO_4^{-2}. Equation (6) shows that a plot of log C versus t should give a straight line, the slope of which equals $k_1/2.303$. It also indicates that the rate constant is independent of the concentration units used. The concentration of SO_4^{-2} at any time can be obtained from the cumulative SO_2 at any time by using the relationship shown in figure 6. The procedure is as follows:

(1) The cumulative SO_2 at various times is obtained by numerical integration of the concentration-of-SO_2-versus-time curve.

(2) The values of the cumulative SO_2, which are in units of ppm hr, are converted to millimols SO_2 by using the definition of ppm and the flow rate of oxygen

TABLE III.—MASS BALANCE RESULTS OF OXIDE-Na_2SO_4 REACTIONS

1	2	3	4	5	6	7	8	9	10	11	12	13
Reactant system	Test duration, hr	SO_4^{-2} applied, mmol	SO_4^{-2} recovered, mmol	SO_4^{-2} reacted, mmol	Fraction SO_4^{-2} reacted	CrO_4^{-2} analysis, mmol	SO_2 evolved, mmol	Ratio of SO_2 evolved to SO_4^{-2} reacted	Calculated $-\Delta W_{SO_3}$, mg	Experimental $-\Delta W$, mg	Calculated ΔW_{Na_2O}, mg	Experimental ΔW, mg
Cr_2O_3 on Cr	2.5	0.0656	0.00385	0.0617	0.94	0.0615	0.0247	0.40	(a)	(a)	(a)	(a)
	120	.0510	0	.0507	1.0	0	.018	.355	(a)	(a)	(a)	(a)
TiO_2 on Pt	29	.169	0	.169	1.0	(a)	.057	.335	13.5	14.3	10.5	10.1

[a]Not applicable.

through the furnace. For a flow rate of 1250 milliliters min^{-1} the conversion factor is $SO_2(mmol) = 3.06 \times 10^{-3}$ $SO_2(ppm\ hr)$.

(3) The millimols of SO_2 evolved are converted to the millimols of SO_4^{-2} reacted by using the relationship given in figure 6, namely, by multiplying by the reciprocal of the slope, 2.86.[5]

(4) The residual millimols of SO_4^{-2} at any time is obtained as the difference between the millimols of SO_4^{-2} reacted and the millimols applied initially.

From the values of residual SO_4^{-2} obtained by this procedure, a plot of log C versus t was constructed for the data of figure 17. The result is shown in figure 18, where we have plotted the negative log SO_4^{-2} (residual) in units of mmol cm^{-2} against time. The data followed a straight-line relationship reasonably well for the first 2 hr, during which 95 percent of the sulfate had reacted. The first-order rate constant obtained from the slope was $k_1 = 1.55\ hr^{-1}$ and is given in table II, where we have also expressed the rate constant in reciprocal minutes. This value can be looked on as the fraction of sulfate reacting each minute, namely, 2.6 percent. It is, however, the fraction of the concentration at the beginning of each minute, which is decreasing with time.

The results for TiO_2 were quite different from those for Cr_2O_3, as shown in figure 19. The specific weight fell at a constant rate throughout the experiment except for an initial period of about 4 hr. It tailed off at 24 hr, at which time the Na_2SO_4 had practically all reacted. In addition, the concentration of SO_2 evolved was practically constant throughout the experiment with an average value of about 0.145 ppm cm^{-2}. The observed weight loss can be correlated with the expected evolution of SO_3 (and SO_2) during the experiment as indicated by reaction (4). In addition, there should be an overall weight gain of the TiO_2–Pt coupon because of the formation of $Na_2O(TiO_2)_n$. The results presented in the last line of table III correlate well with the behavior

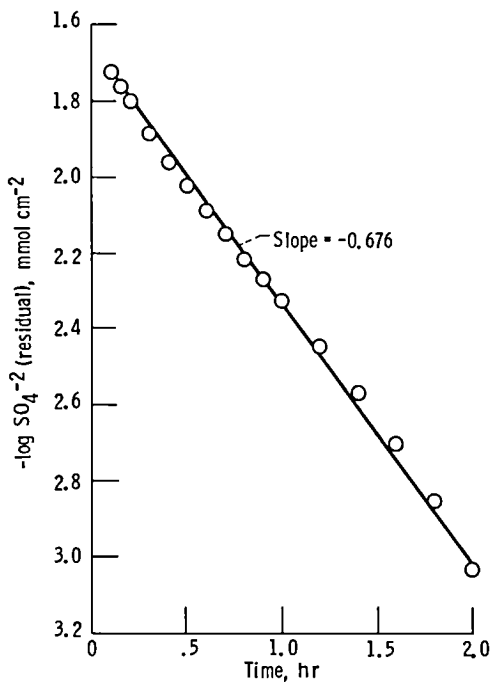

Figure 18.—First-order reaction rate plot for preoxidized chromium specimen corroded at 975° C in flowing oxygen with 3 mg cm^{-2} Na_2SO_4.

predicted by reaction (4). The experiment was run for 29 hr, and analysis of the water-wash solution indicated that all of the SO_4^{-2} applied had reacted (columns 3, 4, and 6 of table III). The cumulative SO_2 evolved (column 8) was compared with the SO_4^{-2} reacted and the proportionality constant obtained was 0.335 (column 9). The total weight loss expected from $SO_2 + SO_3$ evolution during the actual experiment can be calculated from the SO_4^{-2} that reacted. This calculated value is given in column 10 and agrees satisfactorily with the experimental value given in column 11. In addition, the overall weight gain of the platinum coupon after the experiment, resulting from $Na_2O(TiO_2)_n$ formation, was calculated for the amount of SO_4^{-2} that had reacted. The value, given in column 12, agrees very well with the experimental value given in column 13. After the

[5]For the best accuracy the values of the ratio for each experiment were used (i.e., the reciprocals of the values given in column 9 of table III).

experiment the platinum coupon was examined by X-ray diffraction techniques. In addition to the unreacted TiO_2 the compound $Na_2Ti_5O_{11}$ was identified. This is the most stable form of sodium titanate. The compound must be insoluble in water, at least with respect to our extraction technique, because no soluble sodium or titanium was detected in the wash solution from this experiment.

The kinetics of reaction (4) are also quite different from those of reaction (3). The linear weight loss and the practically constant concentration of SO_2 shown in figure 19 are both characteristic of a zero-order reaction: a reaction for which the rate is constant and independent of the concentration of reactants. For this type

$$-\frac{dC}{dt} = k_0 \tag{7}$$

where k_0 is the zero-order rate constant and C is the concentration of sulfate at time t. Integration yields

$$C_0 - C = k_0 t \tag{8}$$

where C_0 is the initial concentration of sulfate. Equation (8) shows that a plot of C versus t should give a straight line whose slope equals k_0. This, of course, is what we have plotted in figure 19. The ordinate is the weight loss due to $SO_3 + SO_2$ evolution. However, as seen in reaction (4), the rate of reaction of SO_4^{-2} and the rate of loss of SO_3 are equivalent, so that the slope of the line in figure 19 represents k_0 for reaction (4). The value of k_0 calculated from this slope is given in table II, where we have used the units mmol cm^{-2} hr^{-1} and also mmol cm^{-2} min^{-1}. The rate constant can also be calculated from the concentration of SO_2, 0.145 ppm cm^{-2}, by using the procedure described previously and the proportionality constant given in table III (column 9). The same value of k_0 is obtained by this method.

The rate constants given in table II can be used to calculate the relative rate of Na_2SO_4 reacting with Cr_2O_3 or TiO_2 during the hot corrosion of IN-738. The comparison is complicated somewhat by the fact that reaction (3) follows first-order kinetics so that the rate at any given time is a function of the concentration of SO_4^{-2} at that time. However, we can determine the SO_4^{-2} concentration on the IN-738 at any time from the smoothed curve of SO_4^{-2} recovered given in figure 3(c). It can also be obtained from the SO_2 evolved (fig. 3(b)) by the method described previously, namely, by calculating the cumulative SO_2 for the desired time and multiplying by the proportionality factor, 2.85. Both methods give comparable results.

We calculated the rates for reactions (3) and (4) at various times during the IN-738 hot corrosion process. We used the first-order constant for Cr_2O_3 given in table II and multiplied the zero-order rate constant for TiO_2 by 7.5 cm^2, a typical area for the IN-738 specimens. The results are given in table IV.

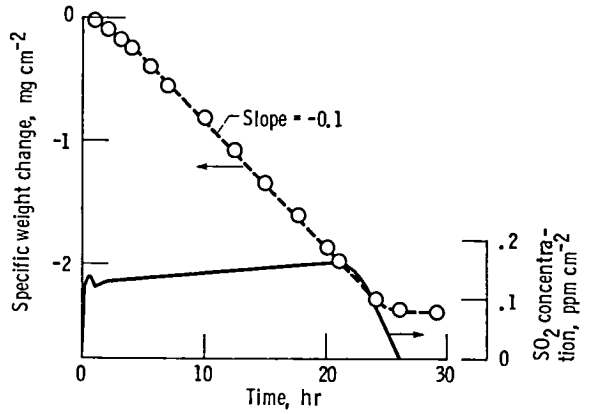

Figure 19.—Specific weight change and concentration of SO_2 evolved as a function of time for plasma-sprayed TiO_2 corroded at 975° C in flowing oxygen with 3 mg cm^{-2} Na_2SO_4. (Sample area, 5.8 cm^2.)

It is obvious that the Na_2SO_4 should react much more rapidly with Cr_2O_3 than with TiO2 on the IN-738 alloy. Initially the Cr_2O_3 rate was a factor of 30 times faster. When the SO_4^{-2} was half gone, after 2.5 hr, the factor was still 15. After 90 percent had reacted, at around 12.5 hr, the reaction with Cr_2O_3 was still three times faster than with TiO_2. The rates did not become comparable until the SO_4^{-2} had practically all reacted. It may therefore be concluded that most of the Na_2SO_4 applied to the IN-738 specimens should react with the Cr_2O_3 in the preoxidized scale.

Rate of reaction of Na_2CrO_4 with TiO_2. – Considerable Na_2CrO_4 was formed in the initial stage of hot corrosion: 0.11 mmol as shown in figure 3(c). The Na_2CrO_4 can evaporate or react with other oxides present on the preoxidized IN-738 specimens. Because TiO_2 is

TABLE IV.—RELATIVE REACTION RATES OF Na_2SO_4 WITH Cr_2O_3 AND TiO_2 DURING HOT CORROSION OF IN-738

Time, hr	Residual SO_4^{-2}, mmol	Fraction of residual SO_4^{-2}	$R(Cr_2O_3)$[a], mmol min^{-1}	$R(TiO_2)$[a], mmol min^{-1}	$\frac{R(Cr_2O_3)}{R(TiO_2)}$
0	0.168	1.0	4.4×10^{-3}	1.5×10^{-4}	29
.5	.135	.80	3.5		23
1.0	.117	.70	3.0		20
2.0	.092	.55	2.4		16
2.5	.085	.50	2.2		15
5.0	.054	.32	1.5		10
7.5	.035	.21	9.1×10^{-4}		6.1
10.0	.025	.15	6.5		4.3
12.5	.017	.10	4.4		2.9

[a]Calculated for a specimen area of 7.5 cm^2.

the most abundant oxide other than Cr_2O_3, the rate of the following reaction was studied:

$$n\ TiO_2 + Na_2CrO_4(l) \rightarrow Na_2O(TiO_2)_n + CrO_3(g) \quad (9)$$

The oxide CrO_3 is very volatile at 975° C (ref. 17) and should volatilize as fast as it is formed. However, because of boundary layer considerations some fraction may be backreflected to the hot specimen (ref. 18). These backreflected CrO_3 molecules would be decomposed on contact with the hot specimen and result in deposition of Cr_2O_3 on the specimen. For these molecules the net reaction would be

$$n\ TiO_2 + Na_2CrO_4(l) \rightarrow Na_2O(TiO_2)_n + 1/2\ Cr_2O_3 + 3/4\ O_2 \quad (10)$$

The specimens used were made by plasma spraying TiO_2 onto platinum coupons as before. They were annealed in oxygen for 2 hr at 975° C before testing. The Na_2CrO_4 was air brushed onto the specimens; about 3 mg cm^{-2} was applied. The reaction was followed with the same techniques used in all of this work.

Several samples were tested for as long as 14 hr. They all exhibited the same behavior: a steady decrease in specific weight similar to that exhibited in figure 19 for the reaction of TiO_2 with Na_2SO_4. The rate of decrease was constant from the beginning of the test until its termination. The rate of weight loss was calculated to be 6.6×10^{-2} mg cm^{-2} hr^{-1}. When corrected for Na_2CrO_4 evaporation, it was 4.1×10^{-2} mg cm^{-2} hr^{-1}. The constant rate of weight loss indicates that the reaction of TiO_2 with Na_2CrO_4 was of zero order like the reaction of TiO_2 with Na_2SO_4. However, neither the rate of weight loss nor the total weight change could be correlated with those calculated for either reaction (9) or (10), because both reactions were occurring simultaneously.

The overall rate of reaction of Na_2CrO_4 can be calculated from the results of the chromium analyses of the water-wash solutions obtained at the end of the experiments. These data gave a value for the rate constant k_0 (analogous to k_0 in eq. (8)) of 9.55×10^{-2} mg cm^{-2} hr^{-1} for Na_2CrO_4 reacting, which is equivalent to 5.9×10^{-4} mmol cm^{-2} hr^{-1} corrected for Na_2CrO_4 evaporation. The value for the rate constant is given in table II for comparison with the rate constant for reaction (4). Using the value of 9.55×10^{-2} mg Na_2CrO_4 cm^{-2} hr^{-1} and the experimental value of the rate of weight loss, 4.1×10^{-2} mg cm^{-2} hr^{-1}, we calculated that 60 percent of the Na_2CrO_4 reacted by reaction (9) and 40 percent by reaction (10); that is, 40 percent of the CrO_3 formed was decomposed back onto the specimen before it could escape through the boundary layer. The overall weight gain of the coupon resulting from $Na_2O(TiO_2)_n$ formation also corroborated these percentages for reactions (9) and (10). As in the reaction with TiO_2 and Na_2SO_4, X-ray diffraction analysis showed the presence of $Na_2Ti_5O_{11}$ on the coupons after the experiment, and the water-wash solutions showed just enough soluble sodium for equivalence to that required for the unreacted Na_2CrO_4.

Chemical Mechanisms

The diverse results obtained in the present studies of the Na_2SO_4-induced hot corrosion of IN-738 can be explained in terms of the following sequence of reactions:

(1) Induction period (0 to 55 hr)

(a) Region of weight loss (0 to 10 hr)—basic fluxing by Na_2SO_4

$$Cr_2O_3 + 2\ Na_2SO_4(l) + 3/2\ O_2 \rightarrow 2\ Na_2CrO_4(l) + 2\ SO_3(g) \quad (3)$$

$$n\ TiO_2 + Na_2SO_4(l) \rightarrow Na_2O(TiO_2)_n + SO_3(g) \quad (4)$$

(b) Region of slow linear oxidation (10 to 55 hr)

$$Na_2CrO_4(l) \rightarrow Na_2CrO_4(g) \quad (11)$$

$$n\ TiO_2 + Na_2CrO_4(l) \rightarrow Na_2O(TiO_2)_n + CrO_3(g) \quad (9)$$

$$2\ Cr + 3/2\ O_2 \rightarrow Cr_2O_3 \quad (12a)$$

$$Ti + O_2 \rightarrow TiO_2 \quad (12b)$$

$$Ni + 1/2\ O_2 \rightarrow NiO \quad (12c)$$

$$Mo + 3/2\ O_2 \rightarrow MoO_3 \quad (12d)$$

$$W + 3/2\ O_2 \rightarrow WO_3 \quad (12e)$$

$$Na_2CrO_4(l) + MoO_3(l)\ (\text{and } WO_3) \rightarrow Na_2MoO_4(l)\ (\text{and } Na_2WO_4(l)) + 1/2\ Cr_2O_3 + 3/4\ O_2 \quad (13)$$

$$Na_2O(TiO_2)_n + MoO_3(l)\ (\text{and } WO_3) \rightarrow Na_2MoO_4(l)\ (\text{and } Na_2WO_4(l)) + n\ TiO_2 \quad (14)$$

$$Na_2WO_4(l) + MoO_3(l) \rightarrow Na_2MoO_4(l) + WO_3 \quad (15)$$

(2) Acceleration period (55 to 60 hr)

$$Na_2O(TiO_2)_n + MoO_3(l) \rightarrow Na_2MoO_4(l) + n\ TiO_2 \quad (16)$$

$$Na_2WO_4(l) + MoO_3(l) \rightarrow Na_2MoO_4(l) + WO_3 \quad (15)$$

(3) Period of rapid linear oxidation (60 to 75 hr)—acidic fluxing

$$Cr_2O_3 + 3\,MoO_3(l) \rightarrow 2\,Cr^{+3} + 3\,MoO_4^{-2} \quad (17a)$$

$$Al_2O_3 + 3\,MoO_3(l) \rightarrow 2\,Al^{+3} + 3\,MoO_4^{-2} \quad (17b)$$

$$Ni + MoO_3(l) \rightarrow NiO + MoO_2 \quad (18a)$$

$$Co + MoO_3(l) \rightarrow CoO + MoO_2 \quad (18b)$$

$$2\,Cr + 3\,MoO_3(l) \rightarrow Cr_2O_3 + 3\,MoO_2 \quad (19a)$$

$$2\,Al + 3\,MoO_3(l) \rightarrow Al_2O_3 + 3\,MoO_2 \quad (19b)$$

$$MoO_2 + 1/2\,O_2 \rightarrow MoO_3(l) \quad (20)$$

(4) Deceleration period (75 hr to end)

$$NiO + Na_2MoO_4(l) \rightarrow NiMoO_4 + Na_2O \quad (21)$$

$$NiO + MoO_3(l)\ (\text{and } WO_3) \rightarrow NiMoO_4\ (\text{and } NiWO_4) \quad (22)$$

$$Na_2O + Ta_2O_5(\text{and } Nb_2O_5) \rightarrow 2NaTaO_3(\text{and } NaNbO_3) \quad (23)$$

These different periods are defined in figure 3(a).

The initial corrosion reactions, which are oxide fluxing reactions, have generally been discussed with reference to thermodynamic stability diagrams of the type first constructed by Pourbaix. We have constructed such diagrams for the Cr-O-S and Ti-O-S systems, superimposed on a diagram for the Na-O-S system, all for a temperature of 975° C (figs. 20(a) and (b)). Similar diagrams for the Mo-O-S and W-O-S systems are also presented in figures 20(c) and (d). The diagrams were constructed by using the FACT computer program (ref. 19). The diagrams show the phases that are in equilibrium with gas mixtures having specified pressures of O_2 and SO_3. As discussed in reference 1, the choice of variables is arbitrary, but precedent has dictated the preference. As a result, to more readily interpret our results with the aid of the diagrams, we have written our reactions involving SO_3 even though species such as SO_2, S_2, $S_2O_7^{-2}$, etc., may be involved. The dashed vertical line in the diagrams is the boundary where the log a_{Na_2O} = log P_{SO_3} in Na_2SO_4 and is representative of "neutral" Na_2SO_4 at 975° C.

Examining the thermodiagrams given in figure 20 shows that the oxides of all four of the elements considered should be converted to the appropriate sodium salts in neutral Na_2SO_4 under 1 atm of oxygen. In addition, the most stable sodium salts under high SO_3 pressure (or low oxide ion activities) were Na_2MoO_4 and Na_2WO_4, with the former being slightly more stable than the latter.

Although these thermodiagrams have been used extensively to interpret hot corrosion behavior in terms of the chemical reactions involved, their usefulness is limited because they give no information on the rates of the reactions or the extent of reaction. Therefore the interpretation of our results is based largely on the results of the kinetic studies described in a previous section.

Induction Period, Region of Weight Loss (0 to 10 hr)

Immediately upon bringing the test specimens to temperature, the Na_2SO_4 melted and started reacting with the Cr_2O_3 to form Na_2CrO_4 and gaseous SO_3, reaction (3). An indication of the early occurrence of this reaction was found in the evolution of SO_2 (fig. 3(b)), in the appearance of water-soluble chromium (fig. 3(c)), and in the rapid drop in residual SO_4^{-2} (fig. 3(c)). This behavior is predicted by the stability diagram for chromium (fig. 20(a)), as noted above, which shows that Cr_2O_3 was not stable in neutral Na_2SO_4 for P_{O_2} down to 10^{-3} atm and that Na_2CrO_4 was the stable phase.

Our rate studies of reaction (3) discussed previously indicate that the Cr_2O_3 should react rapidly with the Na_2SO_4 until all of the Na_2SO_4 is consumed. It appears from the amount of soluble chromium found (fig. 3(c)) that 0.11 mmol of Na_2SO_4 reacted with the Cr_2O_3 in the first 10 hr of hot corrosion. This is considerably more reaction than observed with B-1900 and VIA (ref. 1) where only 0.03 mmol of soluble chromium was found. To put it in perspective, the 0.11 mmol of CrO_4^{-2} found was equivalent to about two-fifths of the Cr_2O_3 on the preoxidized IN-738 sample, or since the liquid Na_2SO_4 slumped to the bottom of the specimens, it was equivalent to removal of all of the Cr_2O_3 from the bottom two-fifths of the specimen.

After an incubation period of about 5 hr the TiO_2 on the specimen began to react with the Na_2SO_4 and formed water-insoluble $Na_2O(TiO_2)_n$, reaction (4). This is evidenced by the drop in soluble sodium beginning at this time (fig. 3(c)). This behavior is also predicted by the stability diagram for titanium (fig. 20(b)) as noted previously. Our kinetic studies also demonstrate that reaction (4) should occur, although comparing the rate with that of reaction (3), given in table IV, indicates that most of the Na_2SO_4 should react with the Cr_2O_3.

Some clarification of the application of the rate studies of Cr_2O_3 and TiO_2 to the initial rate of corrosion of IN-738 is necessary. Comparing the SO_2 concentrations of figure 3(b) for IN-738 and figure 17 for Cr_2O_3 indicates that the reaction with the alloy continued for 20 to 25 hr but the reaction with Cr_2O_3 was effectively completed in 2.5 hr. Obviously the pure Cr_2O_3 reacted more rapidly with the Na_2SO_4 than did the mixed oxide on the IN-738 alloy, which is 75-mol% Cr_2O_3 and 25-mol% TiO_2. The activity of the Cr_2O_3 in the oxide

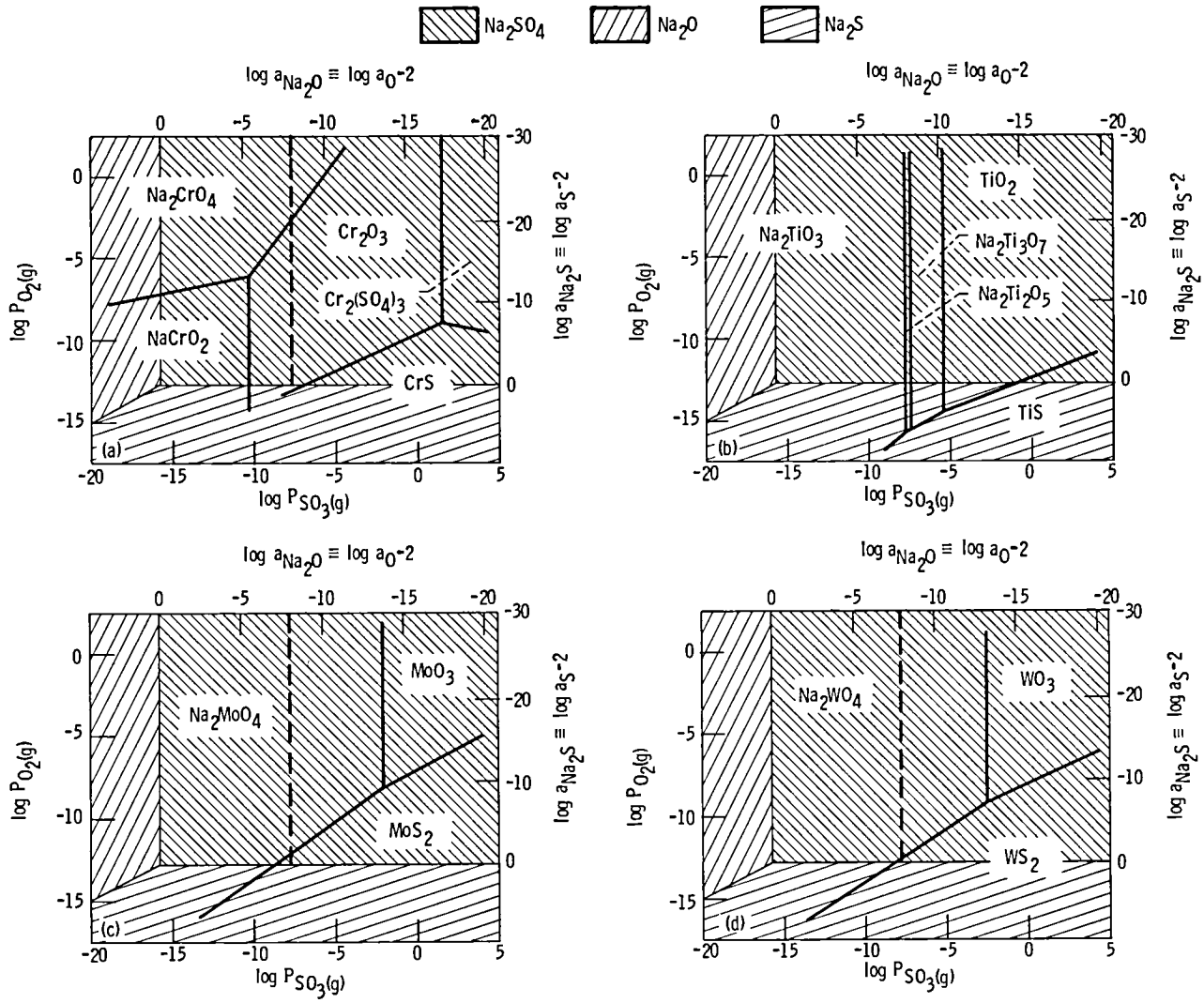

Figure 20.—Thermodynamic phase stability diagrams at 975° C. The Cr-, Ti-, Mo-, and W-O-S diagrams are superimposed on the Na-O-S diagram. The dashed line is drawn where log a_{Na_2O} = log $P_{SO_3(g)}$.

mixture on the alloy was lower than that of the pure Cr_2O_3, and this probably accounts for the difference.

Quantitative interpretation of the IN-738 kinetic data is not possible at this time. It had been hoped that the rate data for the pure oxides Cr_2O_3 and TiO_2 would allow calculation of the rate of reaction of these oxides on the alloy. It appears that kinetic data for known mixtures of Cr_2O_3 and TiO_2 are required. Nevertheless the rate studies with the pure oxides have demonstrated that the rate of reaction of Cr_2O_3 with Na_2SO_4, reaction(3), is much faster than that of TiO_2 with Na_2SO_4, reaction (4), as shown in tables II and IV. In addition, these studies have disclosed the important fact that both oxides continue to react until all of the Na_2SO_4 is consumed.

In any event, the first 10 hr of IN-738 corrosion was a period in which the Na_2SO_4 was mostly consumed by reaction with the protective oxide scale on the alloy, although some sulfide formation can take place. The Cr_2O_3–TiO_2 scale was largely removed from the bottom half of the specimen by this basic fluxing as shown in the micrographs of the 5-hr sample (fig. 8). The weight loss observed during this period resulted from the evolution of considerable amounts of $SO_3 + SO_2$ from the sample during the reactions. Of course, the magnitude of the weight loss and the time at which the minimum in the weight change curve occurred (fig. 3(a)) are functions of the amount of Na_2SO_4 applied and, indirectly, of the thickness of the original oxide scale (ref. 13).

Induction Period, Region of Slow Linear Oxidation (10 to 55 hr)

One result of the rapid reaction between the Cr_2O_3 and the Na_2SO_4 that occurred during the first 10 hr of corrosion was the formation of 0.11 mmol of Na_2CrO_4, as shown in figure 3(c). This large quantity of Na_2CrO_4

was liquid at 975° C and covered the surface of the specimen like the Na_2SO_4 did originally. Examination of figure 3(c) shows, however, that this soluble chromium disappeared rather rapidly between 15 and 30 hr. Concomitantly soluble sodium decreased in a similar manner. Closer examination showed that both species lost about 0.085 mmol between 15 and 30 hr. Because the disappearance was nearly linear over this span of time, we can calculate a disappearance rate, namely, 7.7×10^{-4} mmol cm^{-2} hr^{-1}.

The soluble sodium and chromium can be lost by two main processes at this time: evaporation of Na_2CrO_4 or reaction with TiO_2, reaction (9). We have determined the rates of these two processes, under the conditions of our experiments, and they are given in table II. The sum of the rates of these two processes is 7.4×10^{-4} mmol cm^{-2} hr^{-1}, which is in good agreement with the rate of disappearance of soluble sodium and chromium. We may conclude therefore that the loss of Na_2CrO_4 depicted in figure 3(c) can be largely accounted for by vaporization and by reaction with TiO_2: 20 percent by evaporation; 80 percent by reaction.

Another result of rapid reaction between the Cr_2O_3 and Na_2SO_4 that occurred during the first 10 hr of corrosion was the removal of a large portion of the protective oxide scale. Thereafter the alloy began a long, slow reoxidation that lasted until the end of the induction period, reactions (12). This is shown by the nearly linear weight gain displayed in figures 3(a) and 4 for this time period. It is also evidenced by the thickening of the oxide layer observed in the micrographs of the 20-, 30-, 40-, 48-, and 56-hr samples given in figures 10 to 14. The reformed oxide was not protective in the usual sense even though the rate of oxidation was relatively slow. This is indicated by the fact that the weight increase was nearly linear in time rather than parabolic. The inability of the alloy to produce a protective oxide scale at this time probably resulted from the large depletion of chromium from its exterior areas. The depletion of chromium resulted partly from the preoxidation treatment, as shown in the chromium micrograph of figure 2. However, the situation was markedly aggravated by two additional factors: (1) reoxidation and (2) the formation of sulfides near the bottom of the depletion zone.[6] The chromium micrographs of the 20- and 30-hr samples (figs. 10 and 11) show a 40-μm-wide depletion zone, and the same is true for titanium.

The most important development during this period of reoxidation was the gradual growth of areas of MoO_3-WO_3 along the lower edge of the oxide layer. Soluble molybdenum (MoO_4^{-2}) and tungsten (WO_4^{-2}) were first detected in the water-wash solutions after 10 hr of corrosion, and the quantities continued to increase slowly throughout this period. Originally the soluble species arose from reaction between MoO_3-WO_3 and the considerable quantity of Na_2CrO_4, reaction (13). As the Na_2CrO_4 was converted to $Na_2O(TiO_2)_n$ by reaction (9), the soluble molybdenum and tungsten arose from reaction of the oxides with the $Na_2O(TiO_2)_n$, reaction (14). Some of the recovery of soluble sodium after 40 hr is probably due to this reaction.

The first appearance of MoO_3-WO_3 in the micrographs of the corroded samples was in one area of the 30-hr sample (fig. 11). This sort of area increased in number in the 40- and 48-hr samples (figs. 12 and 13), and an almost continuous such area formed in the latter. The micrographs of these latter two samples show how the MoO_3-WO_3 areas developed. It appears that after the reformed oxide layer reached a thickness of about 30 μm, the underlying Ni-Co islands, which were isolated by the Al_2O_3 tentacles, were leached of all active elements except molybdenum and tungsten. Further oxidation of the specimen effected oxidation of the Ni-Co islands. The molybdenum and tungsten that were dissolved in the islands oxidized also, but these oxides seemed to migrate to the interface between the oxidized islands and the alloy. Sodium was usually found to be associated with the MoO_3-WO_3 areas, although the amount varied from considerable to nearly none as in the area of the 40-hr sample shown in figure 12. The presence of sodium would lower the melting point of the MoO_3-WO_3 because of the formation of Na_2MoO_4-Na_2WO_4 and would also reduce the effective vapor pressure, as discussed in reference 1. Toward the latter part of this period the soluble tungsten started to decrease, probably by reaction (15). This resulted from the slightly greater thermodynamic stability of Na_2MoO_4 as compared with Na_2WO_4 (figs. 20(c) and (d)).

We see that the period from 10 hr to the end of the induction period, 55 hr, is a time in which the alloy slowly reoxidized to form an oxide scale about 60 μm thick. The important characteristics of this oxide are that it is nonprotective and, most importantly, that numerous discrete areas of MoO_3-WO_3/Na_2MoO_4-Na_2WO_4 are formed along the lower edge.

Acceleration Period (55 to 60 hr)

After the long period of linear weight gain the corrosion process began to accelerate at about 55 hr (fig. 3(a)). Simultaneously, the amount of soluble molybdenum markedly increased (fig. 3(c)). This must have resulted from an increase in the rate of formation of Na_2MoO_4 by reactions (15) and (16), probably as a result of the considerable quantity of MoO_3 that had accumulated along the oxide scale. This larger amount of Na_2MoO_4 had a pronounced effect on the morphology of the corrosion samples, because it effected melting of the discrete MoO_3-WO_3/Na_2MoO_4-Na_2WO_4 areas so that

[6] Sulfides can undergo oxidation. The released sulfur diffuses into the alloy and reforms additional sulfides (ref. 20).

they coalesced into a large molten phase.[7] One such area is shown in the micrographs of the 56-hr sample (fig. 14). The molten oxide phase migrated across the sample, disrupting and fluxing the scale above it. In addition, it seemed to be progressing into the alloy itself. The oxide above the MoO_3-WO_3/Na_2MoO_4-Na_2WO_4 was striated and layered in appearance, a typical example of acidic fluxing. However, most of the oxide layer on this sample was still similar to that for the 48-hr sample (fig. 13) with discrete areas of MoO_3-WO_3/Na_2MoO_4-WO_4.

Period of Rapid Linear Oxidation (60 to 75 hr)

Beyond 60 hr the quantity of Na_2MoO_4 increased rapidly, and more and more of the discrete oxide areas merged into large molten masses below the oxide scale. This is shown in the micrographs of the 62-, 68-, and 77-hr samples. In the 77-hr sample (fig. 15) the large molten phase of MoO_3-WO_3/Na_2MoO_4 had finally become a major feature of the scale.[8] This development promoted acidic fluxing of the oxide scale by reactions (17). A major breakup of large areas of the oxide scale occurred and exposed the alloy specimen to the oxidizing atmosphere. Rapid oxidation of the alloy ensued, especially nickel and cobalt, and produced a large porous oxide scale like that shown in figure 4. The rate of oxidation was linear and amounted to nearly 3 mg cm^{-2} hr^{-1}, which was about 20 times faster than the rate observed in the induction period. In addition, it appeared to us that the molten oxide phase attacked the alloy itself, possibly by reactions (18) and (19).[9] Reactions like these were first suggested by Leslie and Fontana (ref. 22) and have been discussed more recently by Peters, Whittle, and Stringer (ref. 23).

The acidic fluxing was self-sustaining and accounted for the linear nature of the attack. The self-sustaining feature resulted from the cyclic operation of reactions (17)[10] and their reverse reactions. After solution of the oxides in the molten MoO_3-WO_3/Na_2MoO_4 phase, reactions (17), the metal cations diffused to the outer zone of the melt, where they were reoxidized by the higher oxygen potential. The cycle kept repeating as the alloy was consumed. The cyclic behavior of acidic fluxing can be explained more quantitatively by the Rapp-Goto model (ref. 25) in which attack is explained in terms of a negative solubility gradient of the corrosion product across the molten phase. The striated appearance of the oxide (fig. 15) is a result of this cyclic nature of the attack. Reactions (18) and (19) can also exhibit a cyclic behavior through reoxidation of MoO_2 at the outer zone of the melt, reaction (20).

As stated previously, evolution of SO_2 was observed during this period of rapid oxidation. It was first detected at about 57 hr, rose to a maximum of 0.014 ppm cm^{-2} (0.1 ppm) at 80 hr, fell off gradually, and approached zero at 115 hr. In all it amounted to around 0.005 mmol. The SO_2 must have resulted from oxidation of the sulfur observed in the molten oxide phase. This conclusion is supported by the observation that the sulfur content of the test specimens dropped from 0.01 mmol for the 50-hr sample to 0.005 mmol for a 75-hr sample.

Deceleration Period (75 hr to End)

At just about 75 hr the corrosion rate decelerated (fig. 3(a)). The magnitude of the deceleration continued to increase with time. This resulted from the conversion of the molten MoO_3-WO_3/Na_2MoO_4 to solid $NiMoO_4$-$NiWO_4$ by reactions (21) and (22) and was accompanied by a rapid decrease in both soluble molybdenum and sodium (fig. 3(c)). These nickel compounds are very stable, and their formation eliminated the molten oxide phase that was causing the acidic fluxing of the alloy specimen. Figure 3(c) shows that the Na_2MoO_4 was reduced to only 0.01 mmol at 90 hr. This value is below that at which the catastrophic attack began at 55 hr. As a result the rate of corrosion was reduced. An area where this transformation occurred is shown in the micrographs of the 90-hr sample (fig. 16). Here $NiMoO_4$-$NiWO_4$ was found along the oxide alloy interface and no evidence of a molten phase was present. In fact, the oxide scale had cracked off at the $NiMoO_4$-$NiWO_4$ phase, which itself was also full of cracks. As stated before, this resulted from an allotropic transformation that occurred upon cooling. Sodium was found deep in the alloy in the carbides with titanium, tantalum, and niobium, reaction (23).

---

[7] Although MoO_3 melts at 800° C, WO_3 melts at 1473° C. The two oxides form an eutectic melting at 770° C. However, the composition at this point is 98-mol% MoO_3 and 2-mol% WO_3 (ref. 21). Only compositions containing more than 70-mol% MoO_3 melt below 975° C, the temperature of our experiments. Because the mol percents of molybdenum and tungsten in IN-738 are 1.0 and 0.8, respectively, it is doubtful that the mixed MoO_3-WO_3 areas would have a composition that would melt. The addition of Na_2MoO_4 or Na_2WO_4, both of which melt below 700° C (ref. 21) would undoubtedly lower the melting points of the mixed MoO_3-WO_3 (ref. 21). Certainly the considerable amounts of Na_2MoO_4 shown in figure 3(c) after 60 hr would lower the melting points below 975° C (ref. 21).

[8] At this stage soluble tungsten had practically disappeared (fig. 3(c)) and most of the sodium was associated with molybdenum.

[9] These reactions are favored thermodynamically. Calculations indicate that the standard free energies at 975° C are negative, especially in the case of Al and Cr: for Al, reaction (19b), $\Delta G = -1060$ kJ mol^{-1}; for Cr, reaction (19a), $\Delta G = -577$ kJ mol^{-1}; for Ni, reaction (18a), $\Delta G = -54$ kJ mol^{-1}; for Co, reaction (18b), $\Delta G = -71$ kJ mol^{-1}.

[10] These reactions are somewhat hypothetical and await substantiation from studies of the MoO_3-WO_3/Na_2MoO_4 system. However, some experimental justification does exist. Bornstein et al. (ref. 24) have shown that Al_2O_3 exhibits an extremely rapid rate of dissolution in molten MoO_3 at 900° C.

Mass Balance

If the loss of Na_2SO_4 observed in these experiments can be ascribed to the processes that we have described, we should be able to account for the Na_2SO_4 at various times during the corrosion process by a mass balance equation. Actually, we are balancing the soluble sodium and the oxide ion, or more simply the Na_2O. The results of such calculations for various times are presented in table V. The calculations are based on the amounts of soluble species given in figure 3(c) and on the rates of evaporation of Na_2SO_4 and Na_2CrO_4 given in table II. All quantities are given in millimols and are characteristic of a specimen area of 7.35 cm^2.

In column 2 we give the amount of SO_4^{-2} recovered, beginning at zero time with the amount originally applied. The quantity of Na_2SO_4 lost by evaporation is given in column 3. This was not continued beyond 10 hr because the Na_2SO_4 had largely reacted by this time and was mixed with a large amount of Na_2CrO_4, which lowered its activity. In column 4 we give the amount of Na_2SO_4 that reacted with Cr_2O_3 , reaction (3), and formed Na_2CrO_4. The CrO_4^{-2} reached a maximum at 10 hr and decreased after that because of vaporization and sequential reactions with other oxides: TiO_2, WO_3, and MoO_3. The loss due to Na_2CrO_4 evaporation is given in column 5. Values have been calculated up to 30 hr, at which time the Na_2CrO_4 was largely consumed. In column 6 we give the amount of Na_2SO_4 that reacted with TiO_2, reaction (4). It was assumed that little reaction took place during the first 5 hr because reaction (4) exhibited an incubation period in our rate studies (fig. 19) and also because the rate of the reaction on the alloy was probably less than that on the pure oxide. Because the Na_2SO_4 was largely used up after 10 hr, the reaction was not considered after that. The value given in column 6 was obtained by measuring the drop in soluble sodium at 10 hr, 0.025 mmol, and subtracting the amount of the 1/2 Na lost by evaporation of Na_2SO_4 and Na_2CrO_4 during this 10 hr, 0.007 mmol + 0.011 mmol = 0.018 mmol.

The main sequential reaction that decreased CrO_4^{-2} was that with TiO_2, reaction (9), which became important at about 15 hr. The amount of CrO_4^{-2} reacting (column 7) was obtained from the drop in the 1/2 Na from time zero by subtracting the 1/2 Na lost by evaporation of Na_2SO_4 (column 3) and Na_2CrO_4 (column 5) and by reaction (4) (column 6). Soluble tungsten (WO_4^{-2}) is given in column 8; it was formed from WO_3 in sequential reactions with Na_2CrO_4 (10 to 40 hr), reaction (13), and with $Na_2O(TiO_2)_n$ (30 to 45 hr), reaction (14). After 45 hr it was lost by reaction with MoO_3, reaction (15). Soluble molybdenum (MoO_4^{-2}) is given in column 9; it was formed in sequential reactions with Na_2CrO_4 (10 to 40 hr), reaction (13); with $Na_2O(TiO_2)_n$ (30 to 75 hr), reaction (16); and finally with Na_2WO_4 (45 to 75 hr), reaction (15). Beyond 75 hr, soluble molybdenum was lost by another sequential reaction with NiO, reaction (21). Concomitantly soluble sodium was lost by reaction (23). The last column, 10, gives the sums of columns 2 to 9 inclusive and should always equal 0.168 mmol, the amount of Na_2SO_4 applied. Although the sums for the different times chosen (except zero time) check fairly well within themselves, their average value is 0.158 mmol, 0.01 mmol less than the amount applied. This discrepancy is not too disturbing if we consider the complexity of the system, the many processes involved, and the inaccuracies inherent in some of the chemical analyses. Actually both Na_2SO_4 and Na_2CrO_4 crept up the platinum hangdown that supported the samples. Corrections for this problem were made, but the accuracy was limited. In addition, in our water-wash procedure the

TABLE V.—SODIUM SULFATE MASS BALANCE

1	2	3	4	5	6	7	8	9	10
Time, hr	Residual Na_2SO_4, mmol SO_4^{-2}	Loss by Na_2SO_4 evaporation, mmol	Reaction (3), mmol CrO_4^{-2}	Loss by Na_2CrO_4 evaporation, mmol	Reaction (4), mmol − 1/2 Na	Reaction (9), mmol − 1/2 Na	Reactions (13) and (14), mmol WO_4^{-2}	Reactions (13) to (16), mmol MoO_4^{-2}	Total, mmol
0	0.168	0	0	0	0	0	0	0	0.168
5	.054	.0035	.10	.005	0	0	0	0	.162
10	.025	.007	.11	.011	.007	0	0	0	.160
15	.011	↓	.105	.016	↓	.008	.001	.004	.159
20	.005	↓	.085	.022	↓	.026	.002	.006	.160
25	.003	↓	.050	.027	↓	.053	.003	.008	.158
30	0	↓	.022	.033	↓	.073	.004	.010	.156
40	↓	↓	.008	.033	↓	.073	.012	.018	.158
50	↓	↓	.004	↓	↓	.071	.012	.022	.156
60	↓	↓	.002	↓	↓	.066	.007	.035	.157
75	↓	↓	0	↓	↓	.051	0	.060	.158
90	↓	↓	0	↓	↓	.101	0	.012	.160

oxide was not removed or abraded, so that small quantities of some deep-lying compounds may not have been dissolved.

The self-consistency displayed by the totals at different times (column 10) is taken as support for the validity of the corrosion mechanism that has been enumerated here and as an indication that no major processes have been overlooked. Some have been included but not discussed, for instance, the formation of the chromium and titanium sulfides observed in the micrographs of the 20-and 30-hr samples. As shown in figure 3(c), sulfur was present even in the 5- and 10-hr samples and increased to 0.01 mmol in the 20- to 50-hr samples. Although this sulfide formation leads to degradation of the alloy, it is thought to be of secondary importance in the overall mechanism. However, it does contribute to the depletion of chromium and the resulting inability of the alloy to form a protective oxide scale during the induction period. Finally the formation of $NaTaO_3$ and $NaNbO_3$, also present in the micrographs of the 20- and 30-hr samples, has not been discussed. This is an important reaction in some alloys, as discussed previously (ref. 26), because $NaTaO_3$ seems to act as a sink for Na_2O and thus inhibits the formation of Na_2MoO_4. However, it has not been effective in this case because of the low concentration, 0.6 mol%, of tantalum and niobium in IN-738.

Conclusions

We have shown that hot corrosion of IN-738 was initiated by basic fluxing of the protective Cr_2O_3–TiO_2 scale and that the fluxing reaction continued as long as Na_2SO_4 was available. Reoxidation of the alloy could not produce a protective scale because chromium was depleted from the exterior surfaces. A long, slow, but linear, oxidation ensued during which MoO_3–WO_3 built up along the oxide-alloy interface. Gradually, MoO_3 reacted with Na_2CrO_4 and $Na_2O(TiO_2)_n$ to form Na_2MoO_4, which lowered the melting point of the MoO_3–WO_3 areas. Large areas of the molten phase MoO_3–WO_3/Na_2MoO_4 were formed, and these areas effected acidic fluxing of the oxide scale and resulted in catastrophic attack of the alloy. Eventually, the attack slowed down as Na_2MoO_4 and MoO_3–WO_3 were converted to their corresponding nickel salts. However, the alloy specimen was largely destroyed by this time.

The Na_2SO_4 had two main effects in this mechanism of hot corrosion: (1) it removed the protective Cr_2O_3–TiO_2 scale; and (2) it supplied sodium that eventually formed Na_2MoO_4, which caused the MoO_3–WO_3 area to melt. Therefore any method of removing the scale should cause hot corrosion if sodium is available; in contrast, if sodium is extracted after scale removal, no hot corrosion should occur. With reference to the first effect, Bourhis and St. John found in Na_2SO_4-induced hot corrosion tests at 900° C that alloys forming a protective Cr_2O_3 layer are not susceptible to accelerated attack. However, if the oxide scale is removed by abrasion, heavy corrosion occurs. We performed tests in which the preoxidation scale was removed by water quenching. The specimen was then coated with 2 mg cm^{-2} of Na_2CrO_4 to supply a source of sodium and to simulate our normal tests. The specimen was oxidized at 975° C and catastrophic hot corrosion occurred in 60 hr, a time not much different from our normal induction period. With reference to the second effect, a normal hot corrosion test was stopped after 10 hr. By this time the protective oxide scale had been largely fluxed. The specimen was cooled and water washed; this removed the Na_2CrO_4 that had formed and any Na_2SO_4 that had not reacted. The oxidation was then restarted and continued for times out to 200 hr. Although a long period of reoxidation ensued, no catastrophic hot corrosion occurred.

The corrosion mechanism postulated herein includes several new ideas and new processes. We have demonstrated that Na_2SO_4 fluxed the Cr_2O_3–TiO_2 scale until all of the Na_2SO_4 was consumed. Generally, it has been believed that reaction (3) resulted in the Na_2SO_4 becoming so "acidic" that the Cr_2O_3 became stable in the Na_2SO_4 and reaction ceased (ref. 27). We have shown that Na_2CrO_4 reacted with TiO_2 to form $Na_2O(TiO_2)_n$ and that both of these compounds reacted with MoO_3–WO_3 to form the low-melting Na_2MoO_4 and Na_2WO_4. We have further shown that acidic fluxing was caused by a molten MoO_3–WO_3 oxide phase containing Na_2MoO_4, instead of a molten Na_2SO_4 phase "acidified" by dissolved MoO_3–WO_3 (ref. 28). In addition, we have suggested that the molten MoO_3–WO_3/Na_2MoO_4 phase can attack the components of the alloy itself by a form of basic fluxing involving MoO_3 and MoO_2.

Two methods of preventing hot corrosion of these alloys that form principally Cr_2O_3 protective scales are suggested by this research: increase the chromium content of the alloy, and *replace* the molybdenum and possibly the tungsten with tantalum or niobium. This latter suggestion has been made previously in references 1 and 26. It appears that in IN-738, in which there is such a small amount of molybdenum to begin with (1.0 mol%), catastrophic corrosion would be eliminated by this replacement.

The application of the corrosion mechanism postulated herein to the problem of hot corrosion of IN-738 in gas turbine engines is complicated by the widely different environmental conditions encountered in service. Although the mechanism is based on laboratory results, we feel that the same processes are involved in practice. However, the relative importance of the various processes may be quite different. Certainly the rate of evaporation of Na_2CrO_4 will be considerably higher in the high-velocity flow environment of a gas turbine. As

compared with our tests, this should decrease the formation of Na_2MoO_4 and lengthen the induction period for catastrophic corrosion. However, the repeated engine cycling and attendant spallation would accelerate chromium depletion and probably shorten the induction period. The most significant and probably the overriding factor is that in an operating gas turbine the Na_2SO_4 in being deposited more or less continuously. If the salt level is high, as in a marine environment, the Na_2SO_4 will probably effect catastrophic hot corrosion. But if the salt level is low, as in a power generating turbine, the high rate of vaporization of Na_2CrO_4 and MoO_3 may prevent catastrophic hot corrosion entirely. A quantitative evaluation of these many complex processes is not possible at this time.

It is necessary to stress the importance of using kinetic data in interpreting hot corrosion processes. To the present time interpretation has been based on thermochemical Pourbaix diagrams. Such diagrams have been invaluable, but, as stated previously, their usefulness is limited because they give no information on the rate of the reactions or the extent of reaction. In addition, the environment in a gas turbine is hardly an equilibrium system. Even if the SO_3 pressure is maintained at some constant value,[11] SO_3 is only one of the products being evolved in the reaction between Na_2SO_4 and Cr_2O_3. The Na_2CrO_4 also evaporates, as we have shown, at a measurable rate of 1.5×10^{-4} mmol cm^{-2} hr^{-1}. In the high-velocity environment of a gas turbine this rate would be increased markedly.

Unfortunately there is little kinetic data available for reactions of the type involved in hot corrosion. Although we have studied three such reactions, reactions (3), (4) and (9), our investigation was limited. The need for more extensive information of this type is imperative to the proper interpretation of hot corrosion phenomena.

National Aeronautics and Space Administration
Lewis Research Center
Cleveland, Ohio, April 3, 1984

[11]Gas turbine combustion gases contain SO_3 at partial pressures between 10^{-6} and 10^{-4} atm depending on the fuel sulfur content. The SO_3 evolved in our tests were equivalent to a partial pressure of 5×10^{-5} to 5×10^{-6} during the course of reaction (3).

References

1. Fryburg, George C.; et al.: Chemical Reactions Involved in the Initiation of Hot Corrosion of B-1900 and NASA-TRW VIA. Electrochem. Soc., vol. 129, no. 3, Mar. 1982, pp. 517-585.
2. Lordi, Francis D.; Foster, Allen D.; and Schilling, William F.: Advanced Materials and Coatings. Gas Turbine Reference Library. GER-2182N, General Electric Co., 1980.
3. Ferguson, J. M.: Hot Corrosion of Some Nickel-Based Alloys in a Laboratory Test (Dean Test). RD/L/N73/80, Central Electricity Research Laboratories, 1980.
4. Page, K.; and Taylor, R. J.: Turbine Corrosion—Rig Evaluation and Engine Experience. Deposition and Corrosion in Gas Turbines, A. B. Hart and A. J. B. Cutler, eds., J. Wiley & Sons, 1973, pp. 350-375.
5. Johnson, D. M.; Whittle, D. P.; and Stringer, J.: Mechanisms of Na_2SO_4-Induced Accelerated Oxidation. Corros. Sci., vol. 15, no. 11/12, 1975, pp. 721-739.
6. Bourhis, Y.; and St. John, C.: Na_2SO_4- and NaCl-Induced Hot Corrosion of Six Nickel-Base Superalloys. Oxid. Met., vol. 9, no. 6, Dec. 1975, pp. 507-528.
7. Fryburg, George C.; Kohl, Fred J.; and Stearns, Carl A.: Hot Corrosion Studies of Four Nickel-Base Superalloys: B-1900, NASA-TRW VIA, 713C and IN 738. Properties of High Temperature Alloys, Z. A. Foroulis and F. S. Pettit, eds., The Electrochemical Society, Inc., vol. 77-1, 1976, pp. 585-594.
8. Erdoes, E.; and Denzler, E.: On the Oxidation and Hot Corrosion of IN 713 LC, IN 738 LC, and IN 939. Behavior of High Temperature Alloys in Aggressive Environments. I. Kirman, et al., eds., Metals Society, 1979, pp. 455-463.
9. Cavalotti, P.; et al.: Some Mechanisms of Scale Degradation in Hot Corrosion Experiments. Behavior of High Temperature Alloys in Aggressive Environments. I. Kirman, et al., eds., Metals Society, 1979, pp. 513-523.
10. Grant, C. J.: Electrochemical Corrosion Measurements on IN 738 and FSX 414 Gas Turbine Alloys in Molten Sulphates. Br. Corros. J., vol. 14, no. 1, 1979, pp. 26-32.
11. Huang, T. T.: An Investigation of Hot Corrosion Mechanisms in Nickel Base Alloys. Ph.D. Thesis, Univ. of Pittsburgh, 1980.
12. Ferguson, J. M.: The Simulation of Hot Corrosion in a Small Burner Rig. RD/L/2113N81, Central Electricity Research Laboratories, 1981.
13. Haque, R.; et al.: Effects of Temperature and Oxide Scale Thickness on the Hot Corrosion of IN-738. High Temperature Materials Chemistry, D. D. Cubicciotti and D. L. Hildenbrand, eds., The Electrochemical Society, Inc., vol. 82-1, 1982, pp. 240-255.
14. Fryburg, George C.; Kohl, Fred J.; and Stearns, Carl A.: Oxidation in Oxygen at 900° and 1000° C of Four Nickel-Base Cast Superalloys: NASA-TRW VIA, B-1900, Alloy 713 C, and IN-738. NASA TN D-8388, 1977.
15. Garlick, Ralph G.; and Lowell, Carl E.: Alloy Composition Effects on Oxidation Products of VIA, B-1900, 713 C, and 738X—a High Temperature Diffractometer Study. NASA TM X-2796, 1973.
16. Kohl, Fred J.; Stearns, Carl A.; and Fryburg, George C.: Sodium Sulfate: Vaporization Thermodynamics and Role in Corrosive Flames. Metal-Slag-Gas Reactions and Processes, Z. A. Foroulis and W. W. Smeltzer, eds., Electrochemical Society, Inc., 1975, pp. 649-664.
17. Stearns, Carl A.; Kohl, Fred J.; and Fryburg, George C.: Oxidation Vaporization Kinetics of Cr_2O_3 in Oxygen from 1000° to 1300° C. J. Electrochem. Soc., vol. 121, no. 7, July 1974, pp. 945-951.

18. Fryburg, George C.; and Petrus, Helen M.: Kinetics of the Oxidating Platinum. J. Electrochem. Soc., vol. 108, no. 6, June 1961, pp. 496-503.
19. Bale, C. W.; Pelton, A. D.; and Thompson, W. T.: F*A*C*T User's Guide. McGill University/Ecole Polytechnique, June 1979.
20. Spengler, C. J.; and Viswanathan, R.: Effects of Sequential Sulfidation and Oxidation on the Propagation of Sulfur in an 85Ni-15Cr Alloy. Metall. Trans. vol. 3, no. 1, Jan. 1972, pp. 161-166.
21. Levin, Ernest M.; Robbins, Carl R.; and McMurdie, Howard F., eds., Phase Diagrams for Ceramists. Vol. I. The American Ceramic Society, 1964.
22. Leslie, W. C.; and Fontana, M. G.: Mechanism of the Rapid Oxidation of High Temperature, High Strength Alloys Containing Molybdenum. Trans. Am. Soc. Met., vol. 41, 1949, pp. 1213-1247.
23. Peters, K. R.; Whittle, D. P.; and Stringer, J.: Oxidation and Hot Corrosion of Nickel-Base Alloys Containing Molybdenum. Corros. Sci., vol. 16, no. 11, 1976, pp. 791-804.
24. Bornstein, N. S.; DeCrescente, M. A.; and Roth, H. A.: The Relationship Between Relative Oxide Ion Content of Na_2SO_4, the Presence of Liquid Metal Oxides and Sulfication Attack. Metall. Trans., vol. 4, no. 8, Aug. 1973, pp. 1799-1810.
25. Rapp, Robert A.; and Goto, K. S.: The Hot Corrosion of Metal by Molten Salts. Second International Symposium on Molten Salts, Jerry Braunstein and J. Robert Selman, eds., Proceedings of the Electrochemical Society, Inc., vol. 81-10, 1979, pp. 159-177.
26. Fryburg, G. C.; Stearns, C. A.; and Kohl, F. J.: Mechanism of Beneficial Effect of Tantalum in Hot Corrosion of Nickel-Base Superalloys. J. Electrochem. Soc., vol. 124, July 1977, pp. 1147-1148.
27. Goebel, J. A.; Pettit, F. S.; and Goward, G. W.: Mechanisms for the Hot Corrosion of Nickel-Base Alloys. Metall. Trans., vol. 4, no. 1, Jan. 1973, pp. 261-278.
28. Giggins, C. S.; and Pettit, F. S.: Hot Corrosion Degradation of Metals and Alloys: A Unified Theory. PWA-FR-11545, Pratt & Whitney Aircraft, June 1979. (AFOSR-79-0905TR, AD-A072645.)

1. Report No.	2. Government Accession No.	3. Recipient's Catalog No.
NASA TP-2319		

4. Title and Subtitle	5. Report Date
Chemical Mechanisms and Reaction Rates for the Initiation of Hot Corrosion of IN-738	July 1984
	6. Performing Organization Code: 505-33-1A

7. Author(s)	8. Performing Organization Report No.
George C. Fryburg, Fred J. Kohl, and Carl A. Stearns	E-1847
	10. Work Unit No.

9. Performing Organization Name and Address	11. Contract or Grant No.
National Aeronautics and Space Administration Lewis Research Center Cleveland, Ohio 44135	13. Type of Report and Period Covered: Technical Paper

12. Sponsoring Agency Name and Address	14. Sponsoring Agency Code
National Aeronautics and Space Administration Washington, D.C. 20546	

15. Supplementary Notes

Published in part in the Journal of the Electrochemical Society, 1984.

16. Abstract

Sodium-sulfate-induced hot corrosion of preoxidized IN-738 was studied at 975° C with special emphasis placed on the processes occurring during the long induction period. Thermogravimetric tests were run for predetermined periods of time, and then one set of specimens was washed with water. Chemical analysis of the wash solutions yielded information about water-soluble metal salts and residual sulfate. A second set of samples was cross sectioned dry and polished in a nonaqueous medium. Element distributions within the oxide scale were obtained from electron microprobe X-ray micrographs. Evolution of SO was monitored throughout the thermogravimetric tests. Kinetic rate studies were performed for several pertinent processes; appropriate rate constants were obtained fro the following chemical reactions:

$$Cr_2O_3 + 2\ Na_2SO_4(l) + 3/2\ O_2 \longrightarrow 2\ Na_2CrO_4(l) + 2\ SO_3(g)$$

$$n\ TiO_2 + Na_2SO_4(l) \longrightarrow Na_2O(TiO_2)_n + SO_3(g)$$

$$n\ TiO_2 + Na_2CrO_4(l) \longrightarrow Na_2O(TiO_2)_n + CrO_3(g)$$

17. Key Words (Suggested by Author(s))	18. Distribution Statement
Alloy; Analysis; Corrosion; Oxidation	Unclassified - unlimited STAR Category 26

19. Security Classif. (of this report)	20. Security Classif. (of this page)	21. No. of pages	22. Price*
Unclassified	Unclassified	33	A03

*For sale by the National Technical Information Service, Springfield, Virginia 22161

NASA-Langley, 1984

National Aeronautics and
Space Administration

Washington, D.C.
20546

Official Business
Penalty for Private Use, $300

THIRD-CLASS BULK RATE

Postage and Fees Paid
National Aeronautics and
Space Administration
NASA-451

NASA

POSTMASTER: If Undeliverable (Section 158
Postal Manual) Do Not Return